https://doi.org/10.5194/essd-2026-465
Preprint. Discussion started: 6 August 2026

TC-SAR-Coast: an event-based Sentinel-1 SAR dataset with high-resolution wind fields for coastal tropical cyclones

Yuting Zhu[1], Yishan Wang[2], Shanshan Mu[3], Yingying Liu[4], Weijia Li[1], Lei Ren[5], Xiaofeng Li[3], and Haohuan Fu[1]

[1]Tsinghua Shenzhen International Graduate School, Tsinghua University, Shenzhen, China
[2]Electronic Information School, Wuhan University, Wuhan, China
[3]Key Laboratory of Ocean Observation and Forecasting and Key Laboratory of Ocean Circulation and Waves, Institute of Oceanology, Chinese Academy of Sciences, Qingdao 266000, China
[4]School of Civil and Environmental Engineering, Cornell University, Ithaca, NY, USA
[5]School of Ocean Engineering and Technology, Sun Yat-sen University, Zhuhai, China

Correspondence: Xiaofeng Li (xiaofeng.li@ieee.org) and Haohuan Fu (haohuan@tsinghua.edu.cn)

Abstract. Coastal tropical cyclones are high-impact events whose nearshore wind structures are difficult to observe with conventional observing systems alone. Available SAR wind products are commonly distributed as scene-level products rather than organized cyclone-focused event records. This fragmentation limits reproducibility, makes quality screening repetitive, and obscures the relationship among storm identity, scene geometry, coastal context, and derived wind fields. We present TC-SAR-Coast, a global event-based Sentinel-1 Level-1 Interferometric Wide Swath (IW) SAR dataset for coastal tropical cyclones from 2015 to 2026. The current release contains 277 tropical-cyclone (TC) events, 411 event-track directories, and 3128 SAR scenes. The dataset is organized into four traceable layers: L0 scene provenance and source linkage, L1 SAR–IBTrACS matchup records, L2 scene-level statistics and hierarchical scene-usability classes, and L3 value-added wind-product files. We develop an event-track-scene data model that preserves provenance, storm context, coastal information, scene usability, and product diagnostics in one hierarchy. Dataset assessment includes completeness and consistency assessment, spatiotemporal coverage analysis, scene-quality statistics, external validation against SFMR, NDBC, and SMAP, and wind-regime-dependent comparison with ECMWF fields. Validation against SFMR aircraft observations demonstrates that the released approximately 1 km L3 wind product captures tropical-cyclone wind fields with high matchup consistency, achieving an RMSE of 3.97 m s^{-1}, bias of -0.36 m s^{-1}, and correlation of 0.82 for the quality-screened matchup sample. TC-SAR-Coast advances SAR tropical-cyclone data use from isolated scene inspection to reproducible event-based analysis by integrating source provenance, storm context, coastal exposure information, quality diagnostics, validation records, and value-added wind fields in a single open archive.

1 Introduction

Coastal tropical cyclones produce severe wind-driven hazards near the ocean–land interface and provide key atmospheric forcing for waves, storm surge, and coastal inundation. Their nearshore surface-wind structure is shaped by storm dynamics, land–sea roughness contrasts, coastal geometry, bathymetric setting, and rapidly changing environmental forcing (Holland,

https://doi.org/10.5194/essd-2026-465
Preprint. Discussion started: 6 August 2026

1980; Emanuel, 1986; Bender et al., 1993; Black et al., 2007; Chen et al., 2021). These interactions can modify eyewall structure, rainband organization, surface-wind asymmetry, and the spatial footprint of damaging winds before, during, and after landfall (D'Asaro et al., 2014; Dare and McBride, 2011; Balaguru et al., 2020). For storm-structure and coastal-hazard applications, the relevant question is therefore not only how intense a storm is at its center, but how its near-surface wind and rainband structures are distributed relative to the coastline (Liu et al., 2019).

Existing observing systems provide complementary but incomplete views of this challenge. Best-track archives such as IBTrACS provide storm identity, positions, and intensity context, but they do not contain pixel-scale ocean-surface observations (Knapp et al., 2010). Reanalysis and operational background fields provide continuous environmental context, but their resolution and smoothing limit their ability to resolve inner-core and coastal gradients (Hersbach et al., 2020). Scatterometers, radiometers, and altimeters provide valuable ocean-surface wind and wave information, but their spatial resolution, land contamination, and sampling characteristics differ from those of coastal SAR scenes (Chou et al., 2013; Manaster et al., 2021; Fore et al., 2018; Ribal and Young, 2019). Aircraft observations such as SFMR are especially valuable for high-wind validation, yet they are available only for selected storms and regions (Uhlhorn et al., 2007; Klotz and Uhlhorn, 2014; Fernandez et al., 2005).

Sentinel-1 SAR helps fill this observational gap by providing high-resolution ocean-surface measurements that can capture storm-scale and coastal-scale structures under cloudy conditions (Torres et al., 2012; Li et al., 2020; Mouche et al., 2026). In tropical cyclones, SAR observations can reveal eyewall-scale high-wind features, rainband organization, wind asymmetry, and coastal exposure patterns that are difficult to infer from coarser sensors alone (Combot et al., 2020; Duong et al., 2021; Avenas et al., 2024a; Shao et al., 2025). The distinctive value of SAR is therefore not only a peak wind estimate, but also the two-dimensional wind footprint, sharp coastal gradients, and storm-relative structure contained in each scene (Zhang et al., 2014; Fan et al., 2020; Zhang et al., 2021; Avenas et al., 2023). However, SAR archives remain fundamentally scene based. A single SAR scene is an instantaneous and partial observation of a moving storm, and its scientific value depends on storm-track context, temporal offset, scene-to-center distance, coastline proximity, land contamination, valid-ocean-pixel support, polarization availability, and retrieval masks. Without these elements, users must repeatedly reconstruct metadata and quality information before analysis.

This creates a data-organization gap between how tropical cyclones are studied and how SAR products are typically accessed. Tropical cyclones are event-based systems with life cycles and evolving tracks, whereas SAR scenes are observation-centric files. Recent ESSD and Scientific Data records emphasize that reusable geophysical archives document representativeness, uncertainty, validation strategy, and task-specific limitations in addition to providing files (Xu et al., 2024; Yang et al., 2025; Gourmelon et al., 2022; Wang and Li, 2021; Derkani et al., 2021; Ribal and Young, 2019). Existing scene-level or demonstration SAR wind products, including tropical-cyclone SAR wind displays, are valuable for scene-by-scene inspection and rapid product visualization (Mouche et al., 2026; Duong et al., 2021). However, they are not designed as unified event-level research archives that preserve uncertainty documentation, validation records, coastal context, and application-ready provenance together. A reusable archive for coastal tropical-cyclone SAR analysis requires a transparent data model, documented selection and matching rules, explicit quality boundaries, and interpretable derived products.

https://doi.org/10.5194/essd-2026-465
Preprint. Discussion started: 6 August 2026

TC-SAR-Coast was developed for this purpose. It organizes coastal tropical-cyclone Sentinel-1 Level-1 IW SAR observations into an event-track-scene hierarchy and stores four linked layers: L0 provenance records, L1 SAR–IBTrACS matchups, L2 scene statistics and hierarchical scene-usability classes, and L3 derived wind-product files. The L3 layer is included because wind fields are a major downstream use of tropical-cyclone SAR observations. It is treated as a value-added, quality-controlled product layer whose uncertainty is evaluated with external references and product masks.

The contributions of this work are as follows. First, we provide a global event-based Sentinel-1 SAR dataset for coastal tropical cyclones from 2015 to 2026, containing 277 TC events, 411 event-track directories, and 3128 scenes. Second, we define an L0–L3 hierarchy that links source provenance, storm matchup metadata, scene usability, and the released L3 wind product. Third, we provide a quality framework combining quantitative scene diagnostics, hierarchical `S/A/B/C` scene-usability classes, and product-level masks. Fourth, we evaluate the dataset with external references and wind-regime-dependent statistics, making the strengths and limitations of the L3 wind field explicit. Fifth, we demonstrate event-scale, coast-relative, and storm-relative scientific-use workflows that convert L3 wind fields and scene metadata into reproducible storm-footprint metrics.

2 Data sources

2.1 Sentinel-1 Level-1 IW SAR observations

Sentinel-1 Level-1 Interferometric Wide Swath (IW) SAR observations are the primary observational input. These Copernicus/ESA acquisitions provide C-band SAR measurements and acquisition metadata relevant to ocean-surface interpretation, including backscatter information, observation geometry, polarization, geolocation, and quality-related fields (Torres et al., 2012; Mouche et al., 2026). TC-SAR-Coast uses each Sentinel-1 Level-1 SAR scene as the canonical scene unit because it preserves the metadata and gridded source fields needed for both scene-level statistics and L3 processing. Each scene is recorded using a unique `scene_id`, acquisition time, scene-center location, orbit information, satellite platform, polarization metadata, and source linkage. The dataset records provenance and derived products for reuse; access to third-party source products remains governed by the original data providers.

Sentinel-1 sampling is not uniform in space or time. The dataset is therefore an event-based observation archive for reproducible SAR analysis rather than a balanced climatological frequency sample. Sentinel-1A and Sentinel-1B availability, acquisition planning, basin-dependent storm occurrence, coastal geometry, and data-access completeness all affect the final sample distribution. The documented sampling characteristics support event studies, retrieval benchmarks, and coastal-exposure analyses with appropriate grouping and filtering.

2.2 IBTrACS best-track records

IBTrACS v04r01 provides event identity, storm positions, basin metadata, storm status, maximum wind, pressure, and track context (Knapp et al., 2010). In TC-SAR-Coast, IBTrACS is used to define event membership and to construct the L1 SAR–

https://doi.org/10.5194/essd-2026-465
Preprint. Discussion started: 6 August 2026

TC matchup records. The matched best-track record supplies storm-center position and intensity context closest to each SAR observation.

IBTrACS is not used as pixel-scale truth for SAR wind retrieval. Best-track records are discrete estimates with agency-dependent uncertainty, whereas SAR scenes are instantaneous spatial samples. The dataset therefore stores IBTrACS variables as storm-context metadata and not as direct validation targets for L3 winds. The scene-selection logic, SAR–TC matching fields, and recommended distance/time filters are described in the Methods section below.

2.3 Coastline and land–ocean mask data

Coastal context is quantified using coastline and land–ocean mask information derived from global shoreline data, including GSHHG-style coastline resources (Wessel and Smith, 1996). These data support coastal-distance calculations, land/ocean separation, land-contamination diagnostics, valid-ocean masking, and product screening. The coastal information is central to the dataset because TC-SAR-Coast focuses on storm observations near coastlines rather than open-ocean cases only. It also enables SAR-specific metrics such as high-wind area within coastal-distance bands and coastal inundation or exposure linkages (Liu et al., 2019).

2.4 ECMWF background fields

ECMWF background winds provide large-scale wind speed and direction context for the L3 processing workflow and technical assessment (Hersbach et al., 2020). These fields are treated as background or prior information rather than independent truth. Comparisons between L3 and ECMWF are therefore described as consistency and regime-dependent difference analyses, not as validation in the same sense as SFMR, NDBC, or SMAP matchups.

2.5 External validation data

Three external reference sources are used for technical evaluation. SFMR aircraft observations provide the primary high-wind reference for tropical cyclones, but their spatial and temporal availability is limited to selected aircraft-sampled storms (Uhlhorn et al., 2007; Klotz and Uhlhorn, 2014). NDBC buoy winds provide independent point-based checks, mainly for nearshore low-to-moderate wind regimes. SMAP L-band radiometer winds provide a coarse-resolution satellite reference for large-scale wind consistency, including tropical-cyclone conditions (Fore et al., 2018; Manaster et al., 2021). These sources have different footprints, sampling intervals, representativeness, and uncertainty characteristics; validation results are therefore interpreted by reference source and wind regime rather than collapsed into a single accuracy number.

https://doi.org/10.5194/essd-2026-465
Preprint. Discussion started: 6 August 2026

3 Methods

3.1 Scene selection and event-based matching

The dataset is constructed as a coastal tropical-cyclone SAR record rather than as a collection of eye-only SAR scenes. Some scenes sample the inner core or eyewall region, whereas others sample outer rainbands, pre-landfall and post-landfall coastal wind structures, or broader storm-environment conditions. Consequently, the full 3128-scene archive is not a uniformly close-to-center validation sample.

Scene-to-storm linkage is made reproducible by storing both qualitative and quantitative matchup information. The L1 records retain the matched IBTrACS time, storm-center position, scene-to-center distance, time difference, matching method, and matchup-quality label. A strict core-analysis subset can therefore be constructed using small `tc_match_distance_km` and `tc_match_time_diff_h` thresholds. Broader coastal wind-exposure or machine-learning subsets can retain scenes at larger storm-center distances when L2 and L3 quality information supports their use. These thresholds are analysis choices rather than hidden archive rules; the released archive preserves the actual quantitative matchup metrics so that users can impose stricter or looser filters transparently.

Filtering choices depend on the intended application. Inner-core tropical-cyclone structure analysis uses `S/A` scenes, SAR-image and L3-mask inspection, and stricter distance and time thresholds. Coastal wind-exposure analysis can also use `B` scenes when coastal context, valid-ocean-pixel fraction, and the L3 valid mask are adequate. External validation follows the independent matchup protocol in Sect. 3.5 rather than L1 storm-center distance alone. Machine-learning applications require event-level or track-level splitting to avoid leakage.

3.2 Event-track-scene hierarchy and L0–L3 data model

TC-SAR-Coast adopts an event-track-scene hierarchy. The event corresponds to a tropical-cyclone identity and year, the track groups SAR scenes associated with a specific event-track collection, and the scene is the Sentinel-1 SAR observation unit. This hierarchy aligns the archive with tropical-cyclone analysis, where users usually begin from a storm event and then inspect available observations.

In this terminology, a TC event is the storm-level unit defined by a tropical-cyclone identity and year, whereas an event-track directory is an internal archive unit that groups one or more SAR scenes associated with a particular collection within that TC event. A single TC event can therefore contain multiple event-track directories. The reported counts of 277 TC events and 411 event-track directories are not alternative estimates of the same quantity; they describe two different levels of the archive hierarchy.

In the released directory structure, each event is stored under TC-SAR-Coast/data/events/<TC_EVENT_ID>/. Track directories are named `track_001`, `track_002`, and so forth. Each track directory contains L0–L3 subdirectories when the corresponding products are available. This design allows a user to move from source provenance to storm matchup, quality screening, and value-added products without reconstructing file relationships.

https://doi.org/10.5194/essd-2026-465
Preprint. Discussion started: 6 August 2026

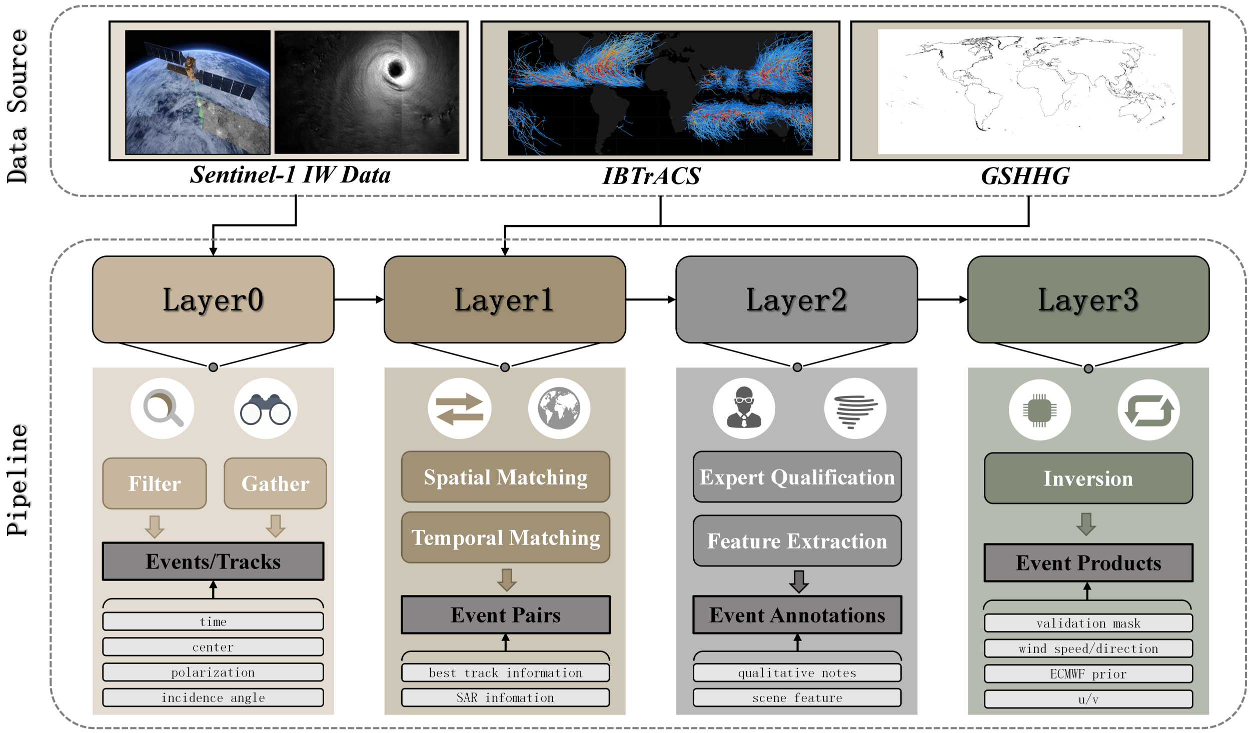

Figure 1. TC-SAR-Coast construction workflow and data hierarchy. Sentinel-1 IW SAR scenes, IBTrACS best-track records, coastline information, ECMWF background fields, and external validation sources are organized into event-track-scene records. L0 preserves scene provenance, L1 stores SAR–IBTrACS matchup information, L2 provides scene-level statistics and hierarchical scene-usability classes, and L3 stores the released value-added wind product with diagnostic masks.

Figure 1 summarizes the data model. The left side of the workflow defines the source inputs: Sentinel-1 IW SAR scenes, IBTrACS best tracks, coastline and land–ocean mask information, ECMWF background fields, and external validation sources. The middle part organizes these inputs into event-track-scene records rather than isolated SAR files. The right side stores the resulting records in four linked layers so that provenance, storm context, scene usability, and the released L3 wind product remain traceable.

The L0 layer records the observational provenance of each SAR scene. It includes `scene_id`, acquisition time, scene-center latitude and longitude, satellite platform, orbit information, polarization metadata, source URL, mean incidence angle, and coastal-distance context. L0 is the preferred entry point for scene discovery and source traceability.

The L1 layer links SAR scenes to tropical-cyclone best-track records. For each scene, the temporally nearest suitable IBTrACS record is retained together with storm identity, center location, intensity descriptors, basin information, and matchup metrics. The most important geometry variables are `tc_match_time_diff_h`, `tc_match_distance_km`, `tc_`

https://doi.org/10.5194/essd-2026-465
Preprint. Discussion started: 6 August 2026

match_method, and match_quality. These fields allow users to filter scenes according to temporal and spatial proximity to the storm.

3.3 Hierarchical scene-quality classification

The L2 layer stores objective scene-level statistics and hierarchical scene-usability annotations. Objective metrics include total pixel count, land and ocean pixel counts, valid VV and VH fractions, robust NRCS statistics, incidence-angle summaries, land fraction, and valid-ocean-pixel support. These metrics are designed for reproducible screening and large-sample analysis, and they provide the quantitative basis for the S/A/B/C scene classes.

The S/A/B/C classes are not intended to be purely subjective labels. They summarize a hierarchy of evidence that combines L1 storm-match geometry, L2 scene statistics, L3 product masks, and expert inspection of SAR interpretability. The L1 evidence describes whether the SAR scene is close enough in time and space to the storm for the intended use. The L2 evidence describes imaging constraints, land fraction, valid-ocean-pixel support, channel availability, and robust backscatter statistics. The L3 evidence describes valid wind-retrieval support, invalid-reason flags, low-coverage or artifact cautions, and the usability of derived wind fields. Expert review is then used to resolve boundary cases and to assess whether the SAR texture contains interpretable tropical-cyclone structure, coastal gradients, or artifacts that require caution.

Class S denotes scenes with exceptional tropical-cyclone structure visibility and high scientific value, suitable for case illustrations and physical structure analysis. Class A denotes high-quality scenes with limited constraints and is generally appropriate for quantitative analysis after standard filtering. Class B denotes usable scenes with moderate limitations; these scenes can support coastal-exposure analysis, machine-learning sample construction, or robustness testing when L1 geometry, L2 metrics, and L3 masks are applied. Class C denotes scenes with substantial limitations, such as strong land contamination, poor storm coverage, low valid-ocean support, or low interpretability; these records are retained for completeness, failure-mode analysis, and transparent filtering but are not intended for unqualified wind-field interpretation. Figure 2 summarizes this hierarchy and the resulting class distribution.

This framework is designed to preserve difficult but informative SAR signatures instead of deleting them. Tropical-cyclone SAR scenes can contain wind-driven roughness patterns, rainband modulation, wave-related structures, land contamination, coastline gradients, and processing artifacts. These features may be nuisance factors for wind retrieval but useful signals for other applications, such as rainband morphology, coastal exposure, or algorithm-stress testing. Following the logic of recent SAR and geophysical image datasets that explicitly distinguish target signatures from look-alikes, ambiguous scenes, and task-specific labels (Yang et al., 2025; Gourmelon et al., 2022; Wang and Li, 2021), TC-SAR-Coast retains low-quality and ambiguous scenes with labels and masks so that users can decide whether to exclude, inspect, or use them for robustness analysis.

3.4 L3 wind-field processing and quality control

The L3 layer provides the released value-added wind product for each scene. It stores gridded wind speed, wind direction, vector components, geographic coordinates, ECMWF background winds, SAR backscatter variables, incidence angle, SAR

https://doi.org/10.5194/essd-2026-465
Preprint. Discussion started: 6 August 2026

Open Access Earth System Science Data Discussions

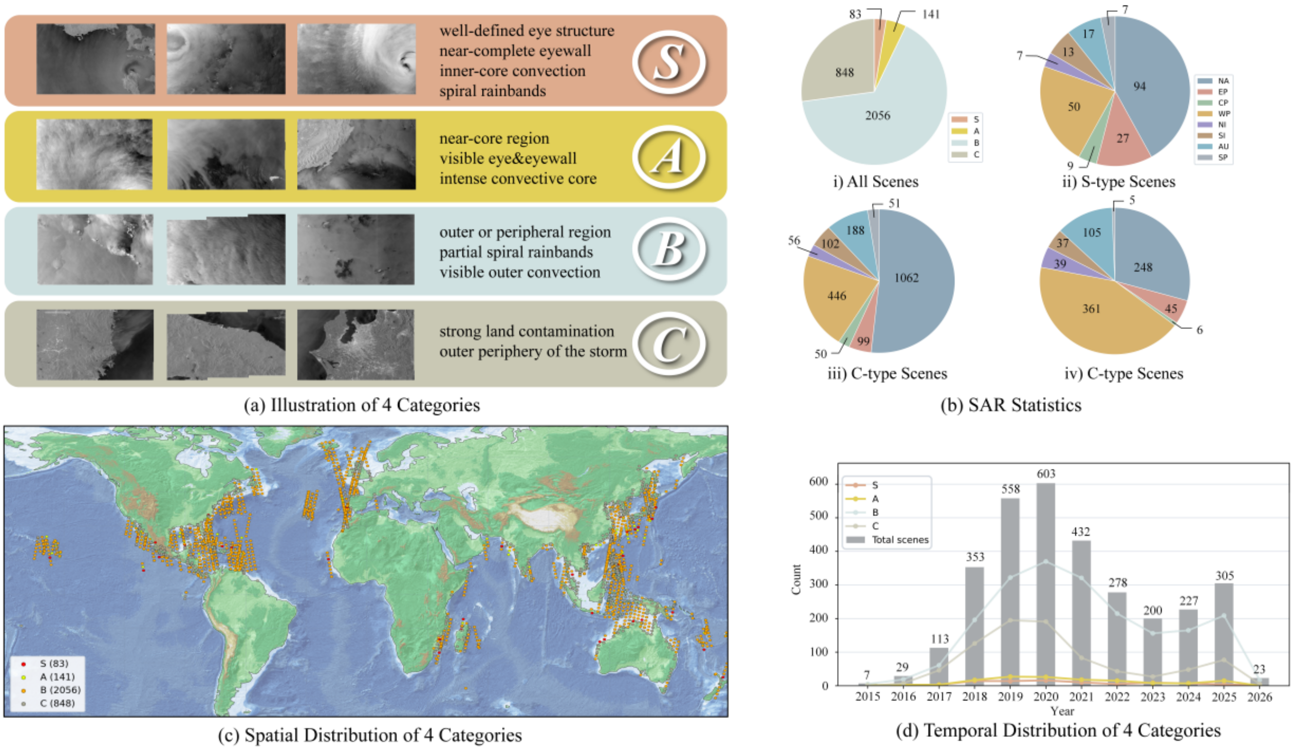

Figure 2. Hierarchical scene-quality framework and dataset-scale distribution. The S/A/B/C classes summarize user-facing scene usability based on storm-match geometry, objective L2 scene metrics, L3 validity information, and expert inspection of SAR interpretability. The classes provide use-specific guidance rather than absolute truth labels.

look direction, ocean masks, valid masks, and invalid-reason flags. The L3 files are designed for quality-aware reuse rather than for unqualified maximum-wind estimation.

The L3 workflow uses Sentinel-1 Level-1 SAR source fields, observation geometry, ocean masking, and ECMWF background information to generate a consistent scene-level wind product on an approximately 1 km grid. The approach follows the broader C-band ocean-wind retrieval context of geophysical model functions, polarization-dependent SAR wind sensitivity, azimuth-cutoff information, and tropical-cyclone-specific high-wind studies (Hersbach et al., 2007; Stoffelen et al., 2017; Zhang et al., 2014; Fan et al., 2020; Zhu et al., 2024; Combot et al., 2020; Duong et al., 2021). Quality control is applied through ocean masks, valid-retrieval masks, invalid-reason codes, and spatial consistency checks. Because ECMWF is part of the product context, ECMWF comparisons are interpreted as prior-background consistency analyses rather than as independent validation. The L3 layer increases the immediate usability of the dataset, with uncertainty information provided through validation tables, wind-regime diagnostics, and product masks.

The released approximately 1 km wind field is the single L3 wind product described in the manuscript. Internal development variants are not presented as separate data products in the main text. The NetCDF variable name is preserved in the data files

https://doi.org/10.5194/essd-2026-465
Preprint. Discussion started: 6 August 2026

and variable dictionary for traceability, and the released field is interpreted together with valid_mask, ocean_mask, qc_flag, and invalid_reason.

3.5 External-validation matchup procedure

External validation is performed with source-specific collocation rules. SFMR matchups use aircraft points within a 180 min temporal window and a 25 km maximum search radius around valid L3 grid cells; this radius is a conservative collocation tolerance rather than the spatial resolution of the SFMR observations. For SFMR, which provides kilometre-scale along-track aircraft observations, the nearest valid observation within the search radius is used, and the SFMR time series is sampled at a 10 s stride to reduce oversampling while retaining storm-scale variability (Uhlhorn et al., 2007; Klotz and Uhlhorn, 2014; Combot et al., 2020). NDBC matchups use point observations within the original short-time matchup window, with the nearest valid L3 grid cell accepted within 25 km. SMAP matchups use same-day scene-footprint or bounding-box comparisons and require at least three valid SMAP pixels; the SMAP value is interpreted as a coarse-footprint median rather than point truth (Fore et al., 2018; Manaster et al., 2021).

For the ECMWF background baseline in the validation figure, the background field is sampled at the same representativeness scale used for each reference source. SFMR and NDBC comparisons use ECMWF wind speed at the aircraft or buoy matchup location, sampled from the collocated L3 grid. SMAP comparisons use the median ECMWF wind speed over valid ocean pixels within the SAR scene footprint, consistent with the coarse-footprint interpretation of the SMAP matchup. These ECMWF statistics are included as a background baseline and are not treated as independent validation of the L3 retrieval.

Outlier handling is applied only for validation summaries and does not remove data from the released L3 products. SFMR summaries exclude points with absolute SAR–SFMR differences larger than 30 m s^{-1} or with robust median-absolute-deviation residuals exceeding 4.5 within the source-method group. NDBC and SMAP summaries use a 25 m s^{-1} absolute-difference threshold and the same robust-z threshold. These filters are intended to remove gross collocation mismatches, land-contaminated samples, and obvious product-reference inconsistencies; all matchup files with outlier flags are retained so that users can reproduce or modify the filtering. This separation between released data and reproducible evaluation filters follows common practice in satellite-wind intercomparison, where scale mismatch and collocation uncertainty must be made explicit (Chou et al., 2013; Ni et al., 2022, 2025).

Validation statistics against SFMR, NDBC, and SMAP are reported as estimate minus reference, where the estimate is either the released L3 product or the ECMWF background baseline. Pixel-level background-difference statistics are reported separately as L3 minus ECMWF. Because the reference systems have different footprints and averaging periods, RMSE and bias are interpreted as matchup-scale statistics rather than intrinsic pixel-level uncertainty.

For the Fig. 5 scatterplot summaries, matchups with reference wind speed below 4 m s^{-1} are excluded to reduce near-calm relative uncertainty and visually unstable low-wind comparisons. This threshold is applied only to the plotted validation summary; the released matchup tables retain the full filtered records and allow users to apply alternative wind-speed thresholds.

The released validation material is designed for reproducibility while respecting third-party data policies. TC-SAR-Coast distributes derived matchup tables, collocation metadata, source identifiers, quality flags, outlier flags, and scripts needed to reproduce the validation summaries. Original SFMR, NDBC, and SMAP observations remain governed by their provider licenses and are referenced through provenance links or source identifiers rather than treated as unrestricted redistributed raw data.

3.6 Completeness and consistency assessment

The final release was checked at the TC event, event-track, scene, L2, annotation, and L3 levels. The complete v3.2 directory contains 277 TC events, 411 event-track directories, 3128 scenes, 3128 L2 metric files, 3128 annotation files, and 3128 L3 NetCDF files. No missing L0 inventories, L1 matchup files, event-information files, L2 metric files, annotations, or required L3 variables remained after the final consistency assessment. Source-specific mask availability and processing choices were recorded in the L2 configuration metadata, including documented fallback handling for older scenes where the original mask variable was unavailable. These records remain traceable and can be filtered by users when land/ocean-mask-dependent analyses require stricter screening.

4 Data records

4.1 Archive organization

TC-SAR-Coast is designed to be accessed in two complementary ways. Event-oriented users can enter the archive through a tropical-cyclone event directory and inspect all Sentinel-1 scenes associated with that event, whereas statistical users can begin from the master scene table and construct filtered subsets across the full archive. This dual access design is important because the dataset is not a random collection of SAR images but an event-linked coastal tropical-cyclone record.

The archive follows an event-track-scene hierarchy. Each event directory contains one or more event-track folders, and each event-track folder contains the L0–L3 records for the SAR scenes associated with that event-track collection. The same `scene_id` is retained across all layers, allowing a user to move from source provenance to storm matching, quality information, and gridded wind fields without relying on file-name inference. The directory structure is:

```
TC-SAR-Coast/
  data/
    events/
      <TC_EVENT_ID>/
        event_info.json
        track_001/
          L0/
            scene_inventory.csv
          L1/
            ibtracs_track.csv
```

https://doi.org/10.5194/essd-2026-465
Preprint. Discussion started: 6 August 2026

Open Access Earth System Science Data Discussions

```
          match_info.json
        L2/
          <scene_id>_l2_metrics.json
          <scene_id>_annotation.json
        L3/
          <scene_id>_l3_wind_v32_qc.nc
```

The same archive can also be accessed through the machine-readable index tables. This table-first route is recommended for statistical analyses, validation subsets, machine-learning sample construction, and cross-event queries:

```
TC-SAR-Coast/
  tables/
    events.csv
    tracks.csv
    scenes.csv  -> l0_path, l2_metrics_path,
                   l2_annotation_path, l3_path
  variable_dictionary.csv
  validation/matchups/
  applications/
```

4.2 Layer contents and traceability

The four data layers separate provenance, storm linkage, quality characterization, and the value-added L3 wind product (Table 1). L0 preserves the SAR source context and coastal information needed for discovery and traceability. L1 records the reproducible connection between each SAR scene and the corresponding tropical-cyclone track state. L2 summarizes scene-level quality and usability information, including the hierarchical `S/A/B/C` classes. L3 provides the gridded wind field and pixel-level masks used for quantitative analysis.

This separation is intended to avoid two common reuse problems. First, users do not need to treat the L3 wind field as a stand-alone product detached from its acquisition and storm context. Second, scenes that are not suitable for one task, such as inner-core wind validation, can still be retained for other tasks, such as coastal wind-exposure mapping or algorithm-development studies, provided that the L1 geometry, L2 quality class, and L3 masks are applied consistently.

4.3 Index tables and variable documentation

In addition to the event directories, the release package contains four machine-readable support records: a master scene table with one row per scene, a file manifest with relative paths and checksums, a variable dictionary for CSV, JSON, and NetCDF records, and an executable example that reproduces the main count, quality, and validation tables. These files are part of the data

https://doi.org/10.5194/essd-2026-465
Preprint. Discussion started: 6 August 2026

Table 1. TC-SAR-Coast layer summary.

Layer	Unit	Main content	Format	Main use
L0	Scene	Source provenance, acquisition geometry, coastal context, source linkage	CSV/JSON	Scene discovery and traceability
L1	Scene–event link	SAR–IBTrACS matchup records, storm context, matchup geometry	CSV/JSON	Event linkage and geometry filtering
L2	Scene	Objective scene statistics and hierarchical S/A/B/C scene-usability classes	JSON	Quality screening and sample selection
L3	Scene	Derived wind fields, background fields, masks, and invalid-reason flags	NetCDF	Quality-aware wind analysis

Table 2. Core record groups and representative variables used for discovery, filtering, validation, and L3 interpretation. The complete release includes a full variable dictionary with data types, units, and file locations.

Record group	Representative variables or fields	Main role	Interpretation constraint
Scene identity and provenance	scene_id, sar_anchor_time, satellite, polarization, source identifiers	Identifies the SAR observation and links all L0–L3 records.	Use scene_id rather than file order for joins.
Storm and coastal context	ibtracs_sid, tc_timestamp, tc_center_lat, tc_center_lon, tc_max_wind_ms, coastal_distance_km	Provides event identity, storm state, and coastal setting.	IBTrACS is context for matching, not pixel-level truth.
Matchup geometry and quality	tc_match_time_diff_h, tc_match_distance_km, match_quality, matching method	Supports transparent filtering by temporal and spatial proximity.	Inner-core analyses require stricter filters than broad coastal subsets.
Scene usability	scene_quality_class, land_fraction, valid_fraction_ocean_vv, incidence_angle_mean	Describes scene-level usability and imaging constraints.	S/A/B/C classes summarize usability but do not replace task-specific screening.
L3 wind and masks	Released approximately 1 km wind field, valid_mask, ocean_mask, qc_flag, invalid_reason	Provides the quality-aware wind product and pixel-selection diagnostics.	Apply masks and diagnostic flags before computing wind statistics.
Background and observation diagnostics	ecmwf_wind_speed, NRCS fields, incidence geometry fields	Supports interpretation of retrieval conditions and regime-dependent comparisons.	ECMWF fields are background context, not independent validation.

record rather than optional bookkeeping. They allow users to verify archive completeness, reproduce the reported 3128-scene inventory, and construct subsets without manually traversing every event directory.

The main variable groups are summarized in Table 2. The table is not a replacement for the full variable dictionary; instead, it identifies fields used for discovery, filtering, L3 interpretation, and external validation. The released L3 wind field is interpreted together with its masks and diagnostic flags. The ECMWF field is retained as background or prior context rather than as an independent validation target.

https://doi.org/10.5194/essd-2026-465
Preprint. Discussion started: 6 August 2026

Open Access Earth System Science Data Discussions

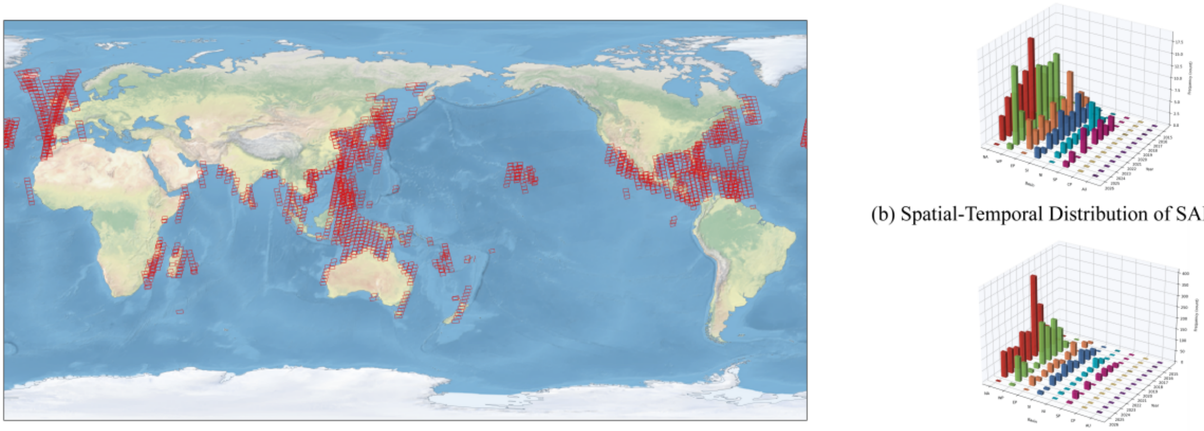

(b) Spatial-Temporal Distribution of SAR Events

(a) Spatial Distrubution of SAR Scenes

(c) Spatial-Temporal Distribution of SAR Scenes

Figure 3. Spatial and temporal coverage of TC-SAR-Coast. The distribution reflects Sentinel-1 acquisition patterns, coastal filtering, and storm occurrence rather than a balanced climatological sampling design.

5 Technical validation and uncertainty

Technical validation is organized around three questions. First, the archive must be complete and internally traceable at the event, track, scene, and layer levels. Second, the quality metadata must expose sample limitations rather than hiding them behind a single usability label. Third, the released L3 wind product must be evaluated with source-aware external references, wind-regime diagnostics, and background-field consistency checks.

5.1 Spatiotemporal coverage

The dataset contains 3128 scenes distributed across 277 TC events and 411 event-track directories. Figure 3 summarizes the spatiotemporal coverage of the archive. The spatial distribution reflects both tropical-cyclone occurrence and Sentinel-1 acquisition planning, with coastal clustering by design. Storm-climatology analyses require explicit treatment of this sampling heterogeneity.

5.2 Scene quality and matchup geometry

Quality statistics are summarized in Table 3. Of the 3128 scenes, 83 are class `S`, 141 are class `A`, 2056 are class `B`, and 848 are class `C`. Median time offset is approximately 0.8 h across all classes, while scene-to-storm distance and land fraction vary strongly by class. This confirms that quality classes capture more than temporal closeness; they also encode storm coverage, coastal contamination, and interpretability.

These statistics also define the representativeness boundary of the dataset. TC-SAR-Coast is rich in event-linked coastal SAR observations, but its distribution is not uniform across basins, storm intensities, coastal settings, or storm-relative locations. The

https://doi.org/10.5194/essd-2026-465
Preprint. Discussion started: 6 August 2026

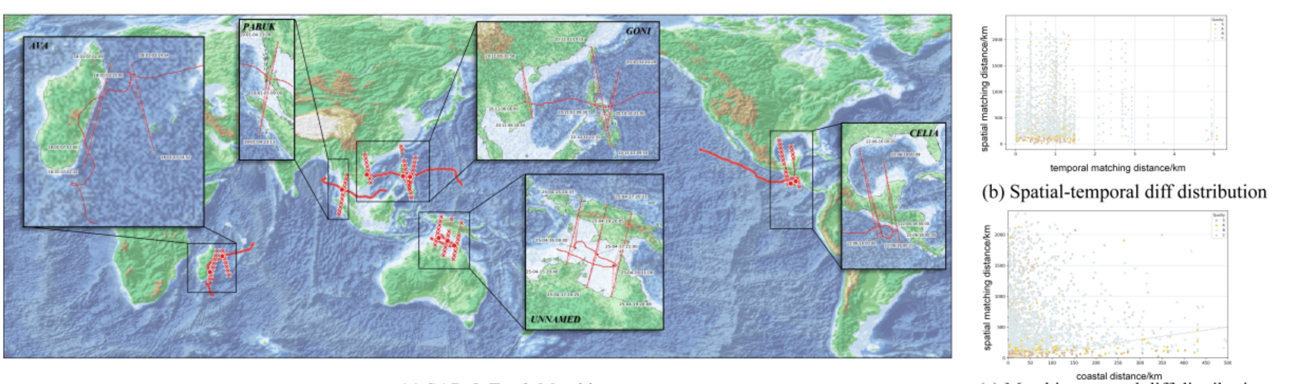

(a) SAR & Track Matching
(b) Spatial-temporal diff distribution
(c) Matching-coastal diff distribution

Figure 4. SAR–IBTrACS matchup geometry. Temporal offset, spatial offset, and coastal context are evaluated together when selecting scenes for analysis.

Table 3. Quality statistics for the final TC-SAR-Coast v3.2 release. Distances are in kilometres, time differences are in hours, and fractions are dimensionless scene-level medians unless otherwise stated.

Metric	All	S	A	B	C
TC event count	277	72	85	235	191
Scene count	3128	83	141	2056	848
Mean TC distance (km)	615.08	117.45	290.87	634.84	696.22
Median TC distance (km)	507.50	76.78	142.50	417.79	630.02
Median time difference (h)	0.80	0.79	0.85	0.79	0.80
Median land fraction	0.09	0.03	0.00	0.02	0.60
Median valid ocean fraction (VV)	0.97	0.97	0.97	0.97	0.94
Median L3 valid-pixel fraction	0.89	0.96	0.96	0.95	0.39

S and A classes are best interpreted as a high-confidence subset for physical storm-structure analysis, whereas the B and C classes expand the archive for downstream tasks that can tolerate or explicitly model imperfect scene conditions. Figure 4 shows the corresponding SAR–IBTrACS matchup geometry and coastal context. This distinction follows the same principle used in event-based climate and tropical-cyclone datasets: the archive must expose how samples were obtained and where they are reliable, rather than implying that all records have equal scientific weight (Xu et al., 2024; Ribal and Young, 2019).

5.3 External validation of the released L3 wind product

Figure 5 summarizes the external validation results for the single released L3 wind product and, for context, the corresponding ECMWF background wind at the same matchup scale. To reduce low-wind relative uncertainty and poorly constrained near-calm comparisons, Fig. 5 includes only matchups with reference wind speed of at least 4 m s^{-1}. Against this quality-screened

SFMR sample, the released L3 product has RMSE of 3.97 m s^{-1}, bias of -0.36 m s^{-1}, and correlation of 0.82 across 33013 matchup points. The ECMWF background sampled at the corresponding aircraft locations has larger SFMR-relative error, with RMSE of 6.35 m s^{-1} and bias of -2.85 m s^{-1}. This comparison shows that the SAR-derived L3 product provides a clear high-wind matchup improvement over the smoother background field in the aircraft-sampled tropical-cyclone cases.

The NDBC and SMAP comparisons sample different spatial scales and wind regimes, but both provide useful independent checks. Against NDBC point observations, the released L3 product has RMSE of 2.58 m s^{-1} and bias of 1.30 m s^{-1}, while the ECMWF background has RMSE of 2.95 m s^{-1} and bias of 0.01 m s^{-1} for the source-specific cleaned sample. Against SMAP, the released L3 product has RMSE of 2.77 m s^{-1} and bias of -0.66 m s^{-1}, compared with an ECMWF-background RMSE of 3.67 m s^{-1} and bias of -1.76 m s^{-1}. These source-aware comparisons show that the released L3 product improves matchup-scale consistency relative to the ECMWF background while also retaining approximately 1 km spatial detail, storm-scale structure, and explicit masks.

The validation is presented as a product assessment rather than as an algorithm-version comparison. Internal development fields are not treated as separate data products in this paper. The released archive contains one quality-controlled approximately 1 km L3 wind product, together with masks, diagnostic flags, and validation metadata. ECMWF is used as the large-scale prior or background field, allowing the added value of the SAR-derived product to be interpreted in terms of higher spatial resolution, sharper coastal and storm-scale gradients, and source-aware matchup performance.

These validation sources are not interchangeable. SFMR is the main high-wind reference but is spatially and temporally limited. NDBC is independent and useful near the coast but has few tropical-cyclone high-wind samples. SMAP provides broad satellite consistency but has a coarser footprint than Sentinel-1. The validation results are therefore reported by source, matchup scale, and wind regime rather than as a single accuracy number.

5.4 Wind-regime-dependent assessment and background consistency

High-wind behavior is critical for tropical-cyclone applications. Figure 6 links two related diagnostics: source-aware validation by SFMR wind regime and pixel-level consistency against the ECMWF background. Panels (a) and (c) show that the released L3 product remains relatively stable from moderate to strong wind regimes, with RMSE of about 3.6–5.5 m s^{-1} across the 15–33 m s^{-1} SFMR reference-wind range and bias close to zero to moderately negative over most of this interval. Above 33 m s^{-1}, the product shows increasing negative bias and larger RMSE, reaching about 6–8 m s^{-1} in the 33–60 m s^{-1} bins. This behavior is reported as an explicit uncertainty boundary for extreme-wind applications rather than as a separate product regime, consistent with previous SAR–SFMR and SAR-derived tropical-cyclone structure studies (Combot et al., 2020; Zhang et al., 2014; Wang et al., 2022; Avenas et al., 2023; Mouche et al., 2026).

Panels (b) and (d) show how the L3 product departs from the ECMWF background across ECMWF wind-speed regimes and how much pixel support is available in each bin. The L3-minus-ECMWF difference is modest in lower and moderate regimes but becomes larger in the high-wind bins, where the SAR-derived field can resolve sharper gradients and localized storm structures than the smoother background field. In the 42–60 m s^{-1} ECMWF wind bin, the L3-minus-ECMWF bias and RMSE are -1.47 and 7.79 m s^{-1}, respectively. Because ECMWF is part of the product context and has its own smoothing

https://doi.org/10.5194/essd-2026-465
Preprint. Discussion started: 6 August 2026

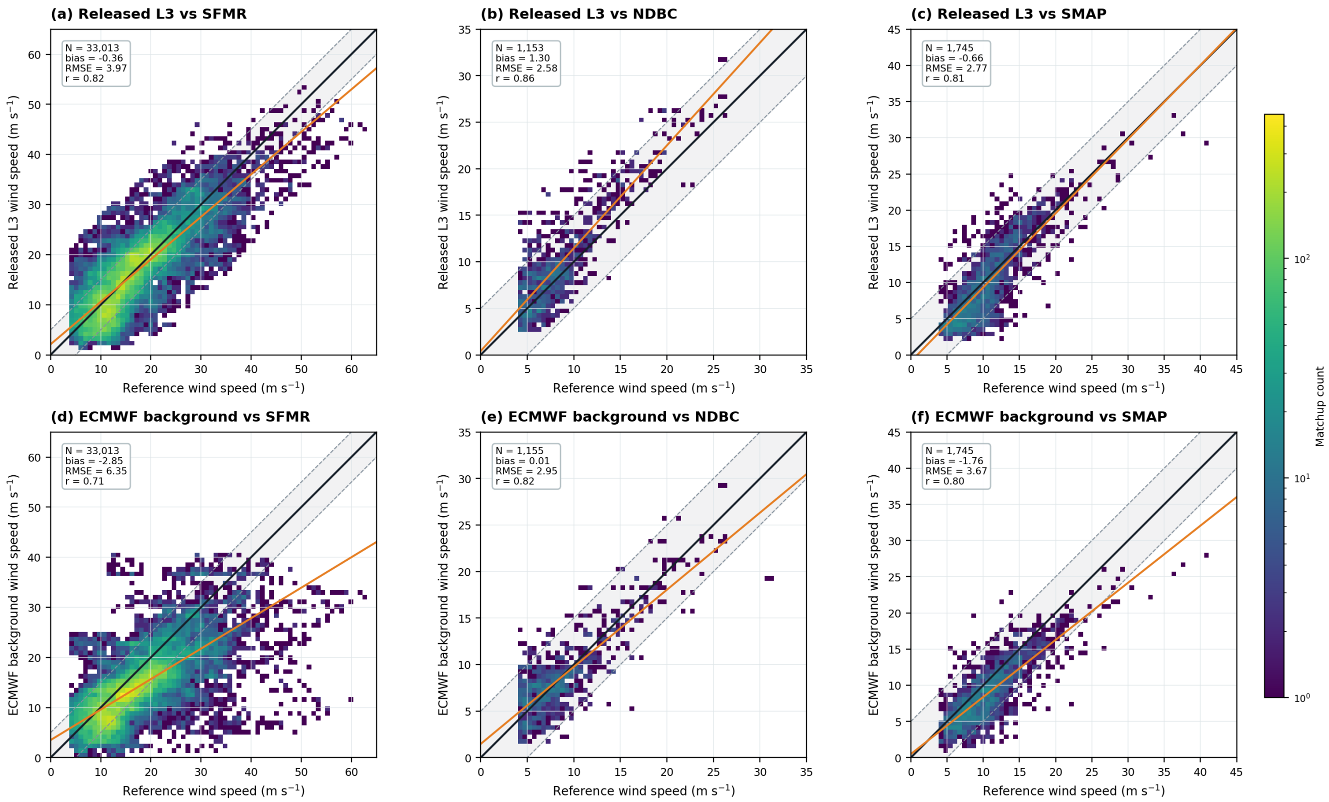

Figure 5. External validation of the released L3 wind product and ECMWF background against SFMR, NDBC, and SMAP for matchups with reference wind speed of at least 4 m s^{-1}. The upper row shows the released L3 wind product against each reference source, and the lower row shows the ECMWF background sampled at the same matchup scale. For SFMR and NDBC, ECMWF values are sampled at the aircraft or buoy matchup locations; for SMAP, ECMWF values are summarized as scene-footprint medians to match the coarse-footprint interpretation. The solid diagonal is the 1:1 line, and the dashed envelopes indicate an illustrative ±5 m s^{-1} difference band. Bias and RMSE are in m s^{-1} and are defined as estimate minus reference.

and position errors, these statistics are used only as a background-difference analysis. Independent accuracy assessment uses SFMR, NDBC, and SMAP matchups with the source-specific caveats described above.

The increase in uncertainty at the highest wind speeds is consistent with known challenges for C-band SAR tropical-cyclone winds, including rain, cross-polarization noise, saturation or flattening of empirical relationships, spatial averaging, storm-motion mismatch, and the scale mismatch between SAR pixels and aircraft observations (Alpers et al., 2016, 2021; Longepe et al., 2022; Combot et al., 2020; Mouche et al., 2026). The L3 product is therefore best used for event-scale wind structure, high-wind footprint, and coastal exposure analyses, while storm intensity, size, and energy diagnostics are interpreted together with established best-track context, parametric/profile concepts, and integrated wind-footprint metrics (Holland, 1980; Chavas and Knaff, 2022; Avenas et al., 2024b).

https://doi.org/10.5194/essd-2026-465
Preprint. Discussion started: 6 August 2026

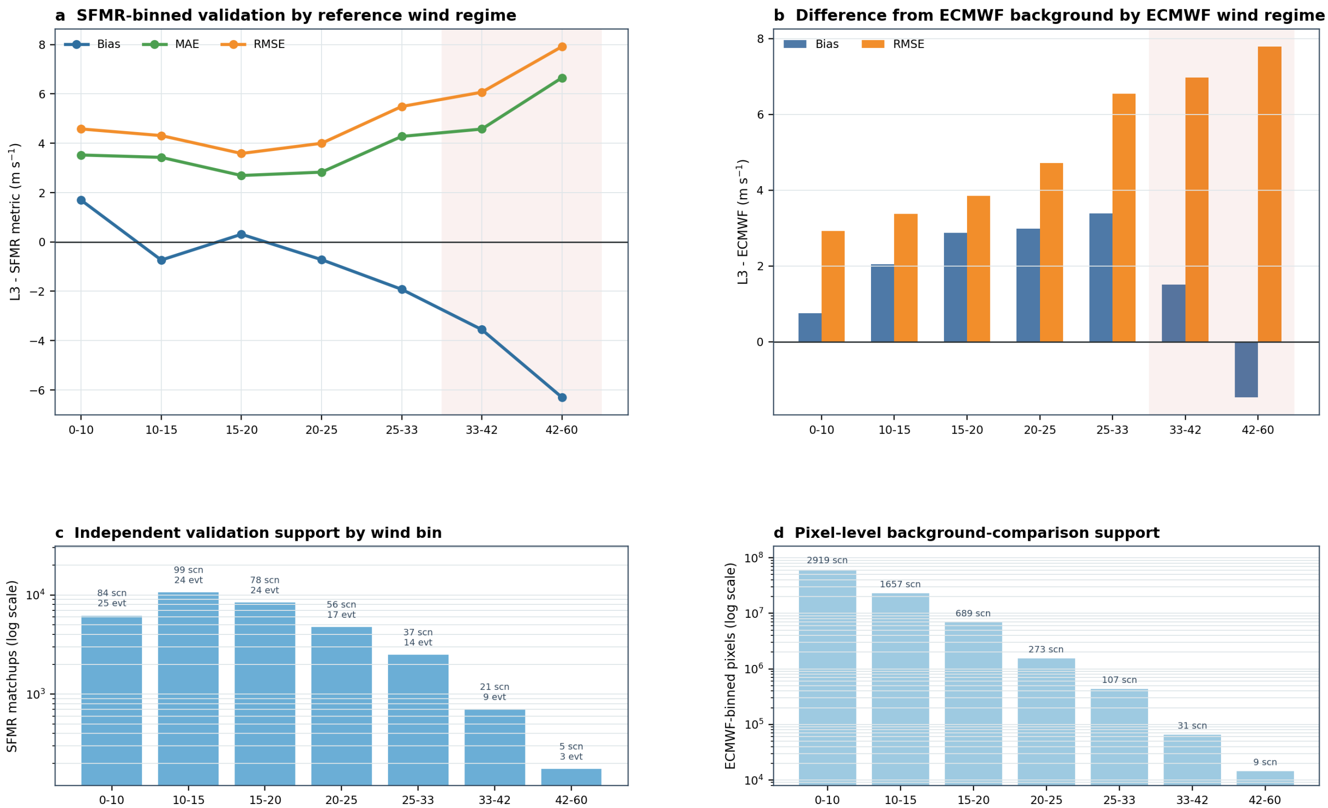

Figure 6. Wind-regime-dependent behavior of the released L3 wind product. Panels (a) and (c) summarize SFMR-binned validation metrics and the corresponding matchup support by reference wind-speed bin. Panels (b) and (d) summarize the difference between the L3 product and the ECMWF prior and the pixel-level support by ECMWF wind-speed bin. Wind-bin labels are in m s^{-1}. The ECMWF comparison describes background-field consistency and SAR-added structure; it is not treated as independent validation.

5.5 Representative L3 product anatomy

Figure 7 illustrates the released L3 product at the scene scale. The source NRCS fields show the SAR information content and possible texture, rainband, or wave-related features, the L3 wind panel shows the quality-masked approximately 1 km wind field with thinned vectors and threshold contours, and the L3-minus-ECMWF panel shows where the released product departs from the large-scale background (Alpers et al., 2016; Fan et al., 2020; Shao et al., 2025). The example presents the product anatomy rather than a separate validation claim; scene-level interpretation uses the L3 wind field together with source fields, masks, and background context.

https://doi.org/10.5194/essd-2026-465
Preprint. Discussion started: 6 August 2026

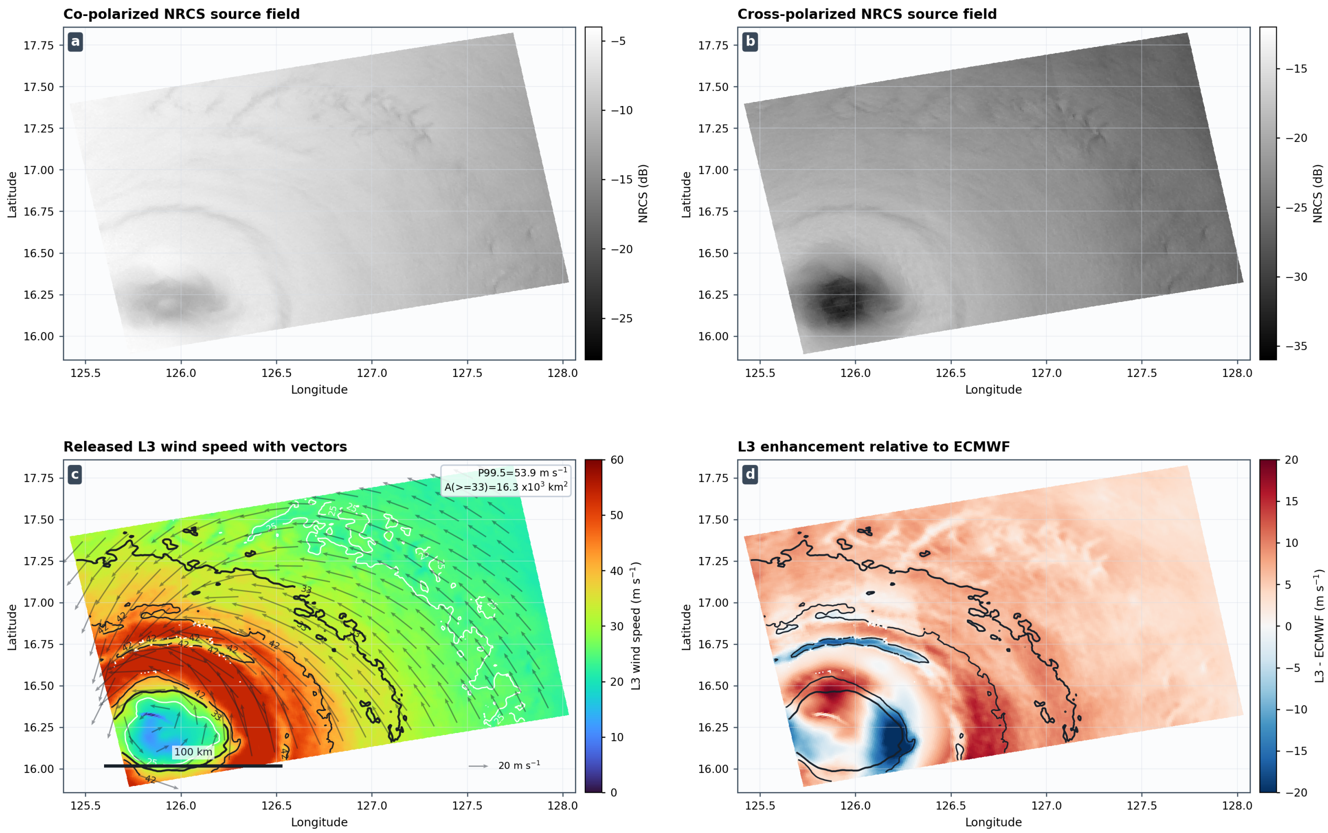

Figure 7. Representative L3 product anatomy showing SAR NRCS source fields, the released quality-masked L3 wind field with thinned vectors and threshold contours, and the L3-minus-ECMWF background difference. Wind-speed contours mark threshold levels used for footprint analysis, and vectors are thinned for readability. The example illustrates the value-added role of L3 and the joint use of source fields, masks, and background context during interpretation.

5.6 High-wind example cases

Figure 8 shows selected high-wind cases used for scientific illustration. These cases were selected from quality class `S/A/B` scenes with sufficient valid-pixel coverage, at least 500 pixels above 33 m s^{-1}, and ECMWF 99th-percentile wind speed above 25 m s^{-1}. They include Surigae (2021), Helene (2024), Harold (2020), Lola (2023), Erin (2025), and Lane (2018). The examples demonstrate that TC-SAR-Coast can support studies of inner-core wind structure, high-wind footprint, and coastal exposure. Interpretation uses percentile-based metrics and high-wind pixel counts rather than single-pixel maximum wind values.

For high-wind applications, robust spatial metrics include the 95th or 99.5th percentile wind speed, the number or area of valid pixels exceeding physically meaningful thresholds, and the location of high-wind regions relative to the coastline and storm center. These metrics are closer to the way tropical-cyclone wind-size products are used in risk and exposure studies

https://doi.org/10.5194/essd-2026-465
Preprint. Discussion started: 6 August 2026

Open Access Earth System Science Data Discussions

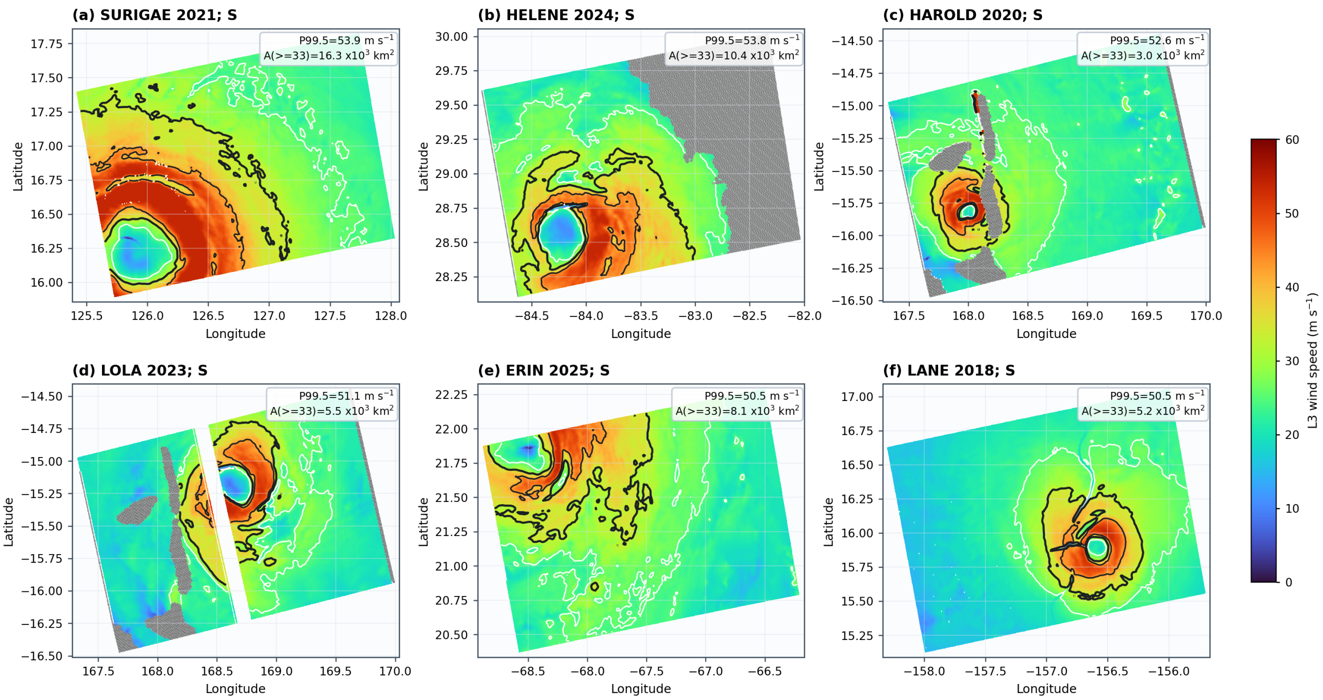

Figure 8. Selected high-wind L3 scenes illustrating storm-scale wind structure in the released product. Colours show quality-masked L3 wind speed and contours indicate high-wind threshold structure; identical colour limits are used to support visual comparison among cases. The cases were selected using scene quality, valid-pixel fraction, high-wind pixel count, and ECMWF high-wind context, and are intended to illustrate product usability rather than to validate single-pixel maximum wind speed.

than single-pixel maxima (Chavas and Knaff, 2022; Xu et al., 2024; Avenas et al., 2024b), and they are less sensitive to isolated retrieval artifacts. In future applications, L3 wind footprints can be summarized using threshold areas analogous to gale-, storm-, and hurricane-force wind extents, while explicitly retaining the SAR-specific masks and uncertainty fields.

6 Discussion

6.1 Dataset value relative to existing products

TC-SAR-Coast is complementary to existing resources. IBTrACS remains the authoritative storm-track context, ECMWF and ERA5 remain large-scale atmospheric references, SMAP and other radiometers provide coarse-resolution storm winds, and scene-level SAR wind displays provide valuable product visualization (Knapp et al., 2010; Hersbach et al., 2020; Fore et al., 2018; Manaster et al., 2021; Mouche et al., 2026). NOAA STAR's SAR tropical-cyclone wind portal, for example, provides SAR-based tropical-cyclone wind products through a practical scene-level web interface (NOAA STAR, 2026). TC-SAR-Coast adds reusable event records with traceable L0–L3 files, scene-quality information, product masks, validation metadata,

https://doi.org/10.5194/essd-2026-465
Preprint. Discussion started: 6 August 2026

and coastal context. These components support reproducible, quality-aware analyses across many storms without rebuilding metadata case by case.

Scene-level displays are commonly optimized for rapid access to selected wind products and visual interpretation (Duong et al., 2021; Mouche et al., 2026; NOAA STAR, 2026). TC-SAR-Coast also includes scenes that do not necessarily capture the eye but are still within the coastal tropical-cyclone environment. These scenes are valuable for studying pre-landfall and post-landfall evolution, outer rainbands, asymmetric wind exposure, coastal hazard-forcing patterns, and SAR-guided improvement of coarser wind products (Zhang et al., 2021; Ni et al., 2025). The broader event-based sampling is used together with matchup, quality, and mask filters.

The added value of TC-SAR-Coast lies in reproducibility, event organization, quality metadata, and validation transparency rather than in a single maximum-wind metric. The archive is designed for repeatable event-based analysis, not only as a catalogue of plotted wind fields. It provides documented multi-storm samples, coastal-distance metrics, quality classes, validation matchups, masks, and reproducible event-level filtering.

6.2 Scientific use cases

The application examples are computed directly from the released L0–L3 records. The first example uses multiple SAR overpasses within one TC event to demonstrate event-scale diagnosis, and the same event is then used for a controlled product-intercomparison benchmark against an external SAR wind product and SFMR aircraft observations. The second converts a nearshore scene into coast-relative exposure metrics and compares the SAR-derived footprint with an ECMWF background field. The third converts an inner-core scene into storm-relative asymmetry metrics and compares the high-wind footprint with the background field. Together, the examples move from event organization and product benchmarking to coastal exposure and storm-structure diagnostics.

The first example is an event-based diagnosis for Delta (2020). Figure 9 combines four SAR overpasses from the same TC event with coastline information, IBTrACS storm position and motion, L3 wind fields, and L3 masks. The sequence shows how an event record can be converted from four scene-level wind products into quantitative event metrics. Within 100 km of the coast, the SAR-observed area exceeding 25 m s^{-1} increases from negligible values on 5 October to approximately 1531, 6656, and 16941 km^2 on 7, 8, and 9 October, respectively. The corresponding area exceeding 33 m s^{-1} appears on 8 October and reaches approximately 3269 km^2 on 9 October. The same event record also supports storm-relative quadrant statistics, with quadrants defined relative to the IBTrACS storm-motion direction. The event-track-scene hierarchy links temporal evolution, coastal exposure, and storm-relative structure within one traceable TC event instead of treating each SAR scene as an isolated image.

Because Delta (2020) also has NOAA STAR tropical-cyclone SAR wind products and SFMR aircraft observations, the same event provides a controlled product-intercomparison case. The event-based archive places different wind products, background fields, and independent observations into a common, reproducible comparison framework. To avoid acquisition-sampling bias, the benchmark uses common Sentinel-1 storm snapshots identified in both resources. Both products are sampled against the same SFMR points, with a ±1 h collocation window, reference wind speed of at least 5 m s^{-1}, and common wind-speed bins.

https://doi.org/10.5194/essd-2026-465
Preprint. Discussion started: 6 August 2026

Open Access Earth System Science Data Discussions

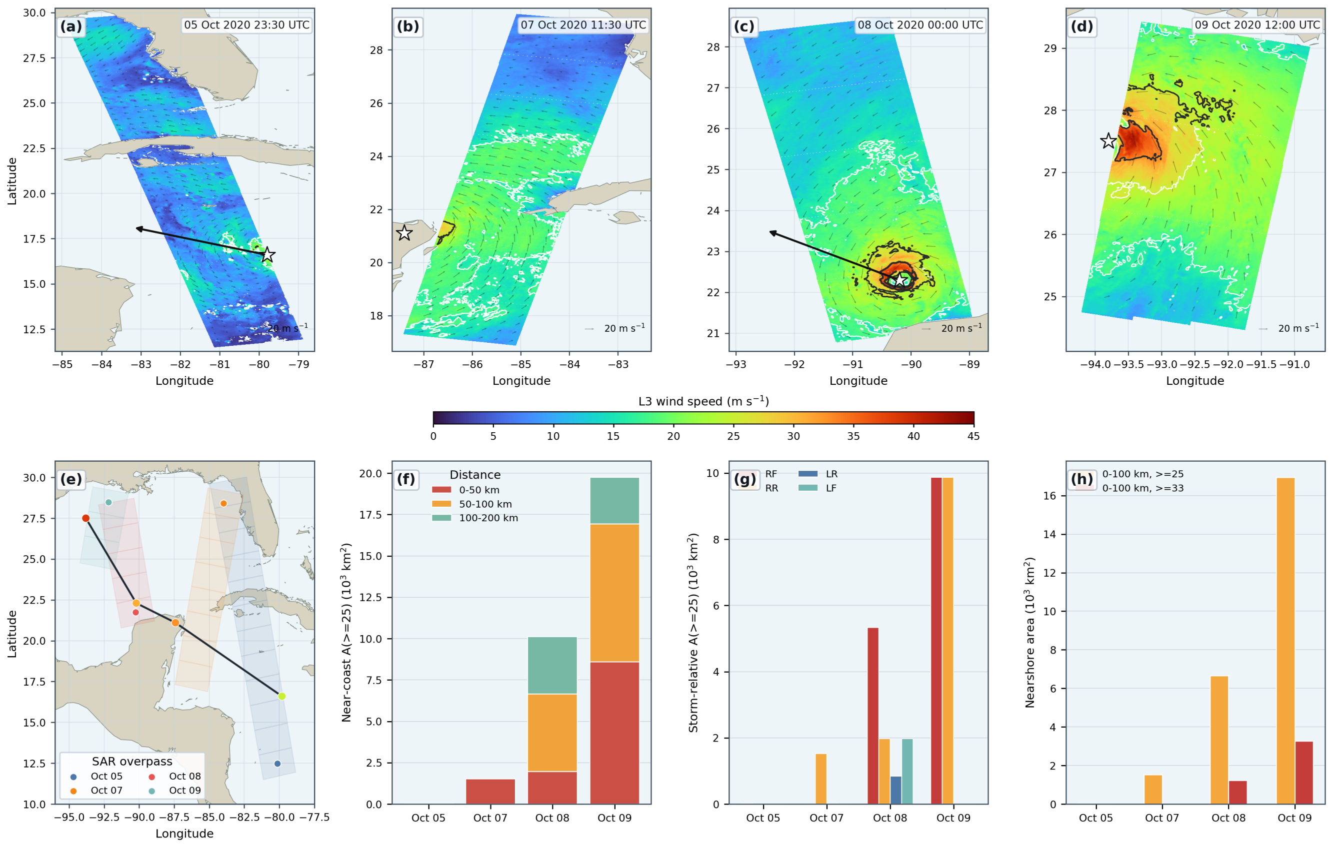

Figure 9. Event-based scientific-use example for Delta (2020). Panels (a)–(d) show four SAR L3 wind fields from the same TC event, with storm centers, motion arrows, wind vectors, and high-wind contours. Panel (e) shows the event overview with the IBTrACS track and true SAR footprint polygons derived from L3 latitude–longitude grid edges. Panel (f) summarizes the valid-ocean area exceeding 25 m s^{-1} by coastal-distance band. Panel (g) summarizes the valid-ocean area exceeding 25 m s^{-1} in storm-relative quadrants; RF, RR, LR, and LF denote right-front, right-rear, left-rear, and left-front quadrants relative to storm motion. Panel (h) summarizes the 0–100 km nearshore area exceeding 25 and 33 m s^{-1}. Areas are approximate grid-cell areas over valid ocean pixels.

Figure 10 shows that the TC-SAR-Coast L3 product is comparable to the NOAA STAR SAR wind product for this case and has lower RMSE in the 17–25, 25–33, and $\geq$33 m s^{-1} bins, while both SAR-based products substantially outperform the ECMWF background at high wind speeds. For the full set of 17013 SFMR matchups, the bin counts are 5123, 9602, 1475, and 813 for 5–17, 17–25, 25–33, and $\geq$33 m s^{-1}, respectively. The corresponding RMSE values for TC-SAR-Coast are 4.15, 2.07, 3.23, and 5.24 m s^{-1}; for NOAA STAR they are 4.48, 3.26, 5.22, and 6.54 m s^{-1}; and for the ECMWF background they are 5.47, 3.51, 6.64, and 10.05 m s^{-1}. This case-level result provides a controlled Delta-event benchmark for product comparability against independent aircraft data.

https://doi.org/10.5194/essd-2026-465
Preprint. Discussion started: 6 August 2026

Open Access Earth System Science Data Discussions

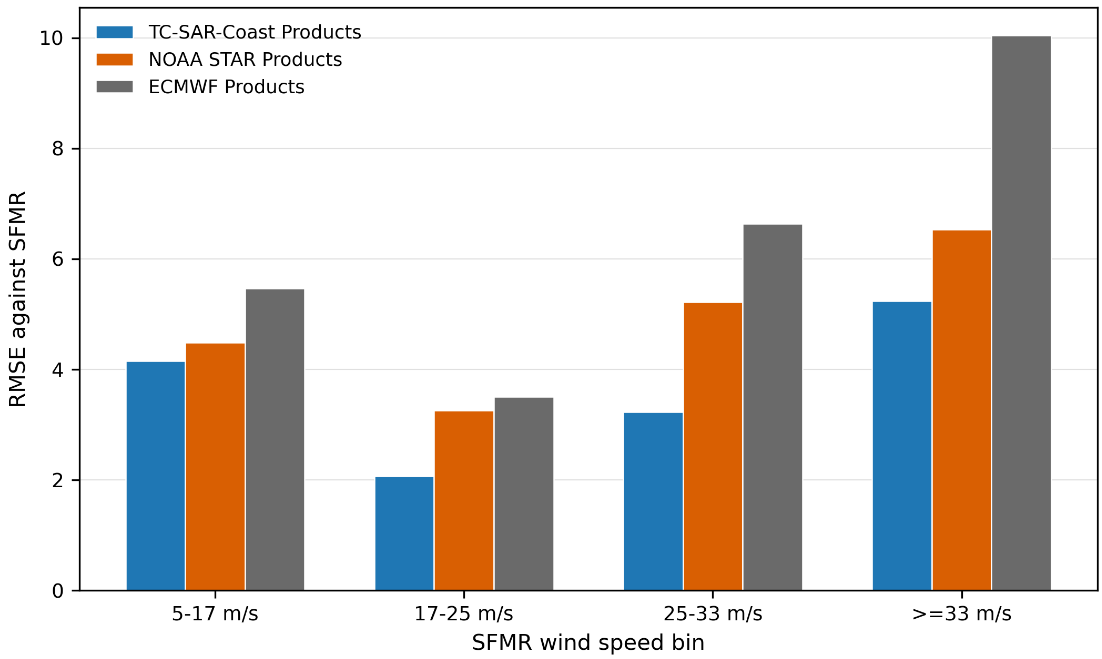

Figure 10. Case-level product intercomparison enabled by the event-based Delta (2020) archive. RMSE is computed against SFMR aircraft observations by reference wind-speed bin for the TC-SAR-Coast L3 product, the NOAA STAR SAR wind product, and the ECMWF background field. The benchmark uses common Sentinel-1 storm snapshots and the same SFMR points, with a ± 1 h time window and SFMR reference wind speed of at least 5 m s^{-1}.

The second example is coastal high-wind exposure forcing. For Veronica (2019), Fig. 11 combines the released L3 wind field, L3 ocean mask, ECMWF background winds, and coastline-relative distance to summarize high-wind valid-ocean area within coastal-distance bands. Within 100 km of the coast, the scene contains approximately 23989 km^2 of valid-ocean area exceeding 25 m s^{-1} and approximately 9581 km^2 exceeding 33 m s^{-1}. These values are approximate grid-cell areas rather than inundation extents, but they illustrate a reproducible way to convert SAR wind scenes into coast-relative exposure metrics that can later be coupled with bathymetry, surge models, SAR inundation mapping, or wind–wave observational datasets (Liu et al., 2019; Li et al., 2002; Ribal and Young, 2019; Derkani et al., 2021).

The third example is storm-relative high-wind footprint analysis. Figure 12 uses Surigae (2021) to convert a SAR wind image into quadrant-resolved footprint metrics relative to the IBTrACS storm-motion direction. Within the valid SAR footprint, the released L3 product contains approximately 16334 km^2 of valid-ocean area above 33 m s^{-1} and 7074 km^2 above 42 m s^{-1}. The right-front quadrant alone contains approximately 11850 km^2 above 33 m s^{-1}, showing how TC-SAR-Coast can support quantitative studies of wind asymmetry, eyewall-scale structure, SAR-based wind-size metrics, and links to air–sea or ocean-response diagnostics while avoiding reliance on single-pixel maximum wind speed (Zhang et al., 2021; Shao et al., 2025; Avenas et al., 2024a; Combot et al., 2024; Zhang et al., 2024).

https://doi.org/10.5194/essd-2026-465
Preprint. Discussion started: 6 August 2026

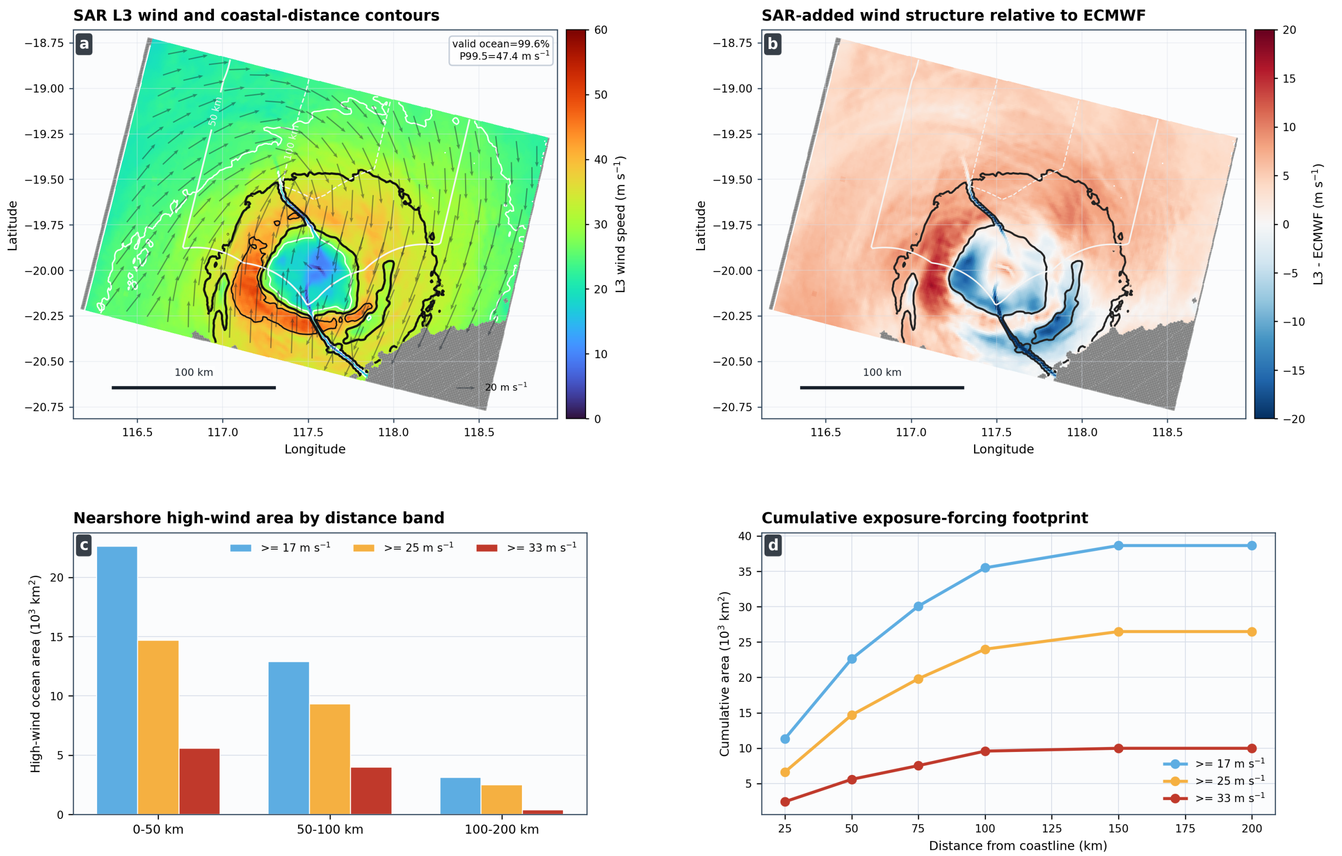

Figure 11. Application case for coastal high-wind exposure forcing using Veronica (2019). The upper panels show the released L3 wind field, coastal-distance contours, and the spatial difference from the ECMWF background for this nearshore scene. The lower panels summarize high-wind valid-ocean area by coastal-distance band and cumulative distance from the coastline. Areas are approximate grid-cell areas over valid ocean pixels. The example quantifies wind forcing relative to the coast; it is not a direct inundation map.

Together, these examples clarify the distinction between TC-SAR-Coast and display-oriented SAR wind products. A plotted SAR wind field is useful for visual inspection, but the event-track-scene hierarchy, L0 coastal context, L2 quality information, L3 masks, and validation metadata allow scenes and events to be converted into reusable metrics such as nearshore high-wind area, event-scale exposure evolution, storm-quadrant wind footprint, or controlled product intercomparison against independent aircraft data. These metrics are computed from traceable L0–L3 records, masks, and scene metadata rather than manually interpreted from plotted images. The same structure can later be extended to wind–wave or wave–current questions because SAR has a long history of supporting ocean-wave, swell, and surface-dynamics interpretation (Li et al., 2002; Engen and Johnsen, 1995; Chapron et al., 2005; Ardhuin et al., 2009; Collard et al., 2009; Li et al., 2020; Quach et al., 2021; Pouplin et al., 2024; Kleinherenbrink et al., 2024).

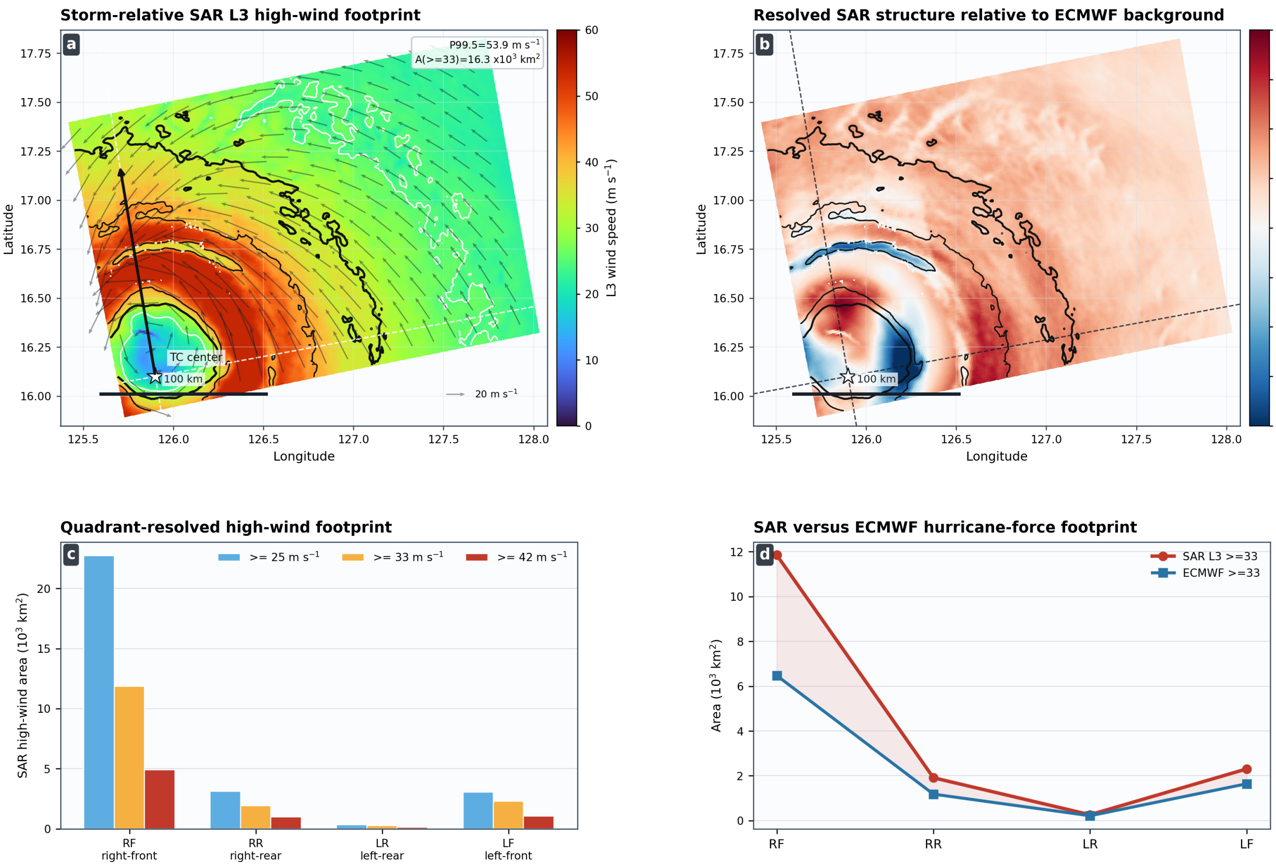

Figure 12. Application case for storm-relative high-wind asymmetry using Surigae (2021). The upper panels show the released SAR L3 wind field, storm center, motion-relative quadrant axes, and the spatial difference from the ECMWF background for this inner-core scene. The lower panels convert the same scene into quadrant-resolved high-wind areas and compare the 33 m s^{-1} footprint with the ECMWF background. Quadrants are defined relative to the IBTrACS storm-motion direction, and areas are valid-ocean grid-cell areas within the SAR footprint.

Table 4 summarizes broader analysis pathways enabled by the dataset. These are not presented as completed process studies in this data paper; rather, they specify how the released layers can be combined to support reproducible downstream science. The examples and pathways demonstrate that the dataset is documented and quality-controlled for multiple scientific questions, while full process attribution remains the subject of future application studies (Xu et al., 2024; Yang et al., 2025; Gourmelon et al., 2022; Wang and Li, 2021; Derkani et al., 2021).

6.3 Limitations

The main limitations are those expected for an event-based SAR archive. Sentinel-1 sampling is opportunistic and uneven, so the archive should not be treated as a climatological storm-frequency sample. Each SAR scene is instantaneous and spatially

https://doi.org/10.5194/essd-2026-465
Preprint. Discussion started: 6 August 2026

Table 4. Example scientific analysis pathways supported by TC-SAR-Coast and the safeguards required for each use.

Analysis pathway	Required dataset layers	Recommended metrics	Main safeguard
High-wind footprint and wind-size analysis	L1 storm context, L2 quality, L3 wind fields	Area or pixel count above 17, 25, and 33 m s^{-1}; p95 and p99.5 wind speed; storm-relative quadrants	Avoid single-pixel maximum wind; use masks and quality classes.
Coastal exposure before and after landfall	L0 coastal distance, L1 timing, L2 land fraction, L3 valid winds	High-wind area within coastal-distance bands; valid-ocean fraction; event-relative acquisition time	Separate coastal signal from land contamination and scene coverage limits.
SAR retrieval benchmarking	L2 NRCS statistics, L3 wind fields, SFMR/NDBC/SMAP matchups	Bias, RMSE, MAE, correlation by wind bin, basin, quality class, and reference source	Do not mix reference sources without scale-aware interpretation.
Machine-learning sample construction	L0–L3 master tables and quality labels	Event-level train-test splits; class balance; mask-aware loss or evaluation	Avoid leakage from random scene-level splitting.

partial, so storm-track context and acquisition timing are essential for interpretation. The hierarchical `S/A/B/C` classes summarize scene usability, but they are designed to guide rather than replace task-specific screening.

For L3 wind use, the relevant uncertainty sources include SAR noise, rain effects, land contamination, background-field dependence, collocation mismatch, and increasing uncertainty at extreme wind speeds (Alpers et al., 2016, 2021; Uhlhorn et al., 2007; Klotz and Uhlhorn, 2014; Combot et al., 2020; Mouche et al., 2026). These limitations are handled through masks, diagnostic flags, validation tables, and recommended filtering rather than by removing difficult scenes from the archive. The released L3 wind field is a quality-aware spatial product and is not intended as an unqualified estimate of storm maximum intensity.

7 Usage notes

Recommended entry points depend on the intended task. Event case studies begin with `event_info.json`, L1 matchup records, and L2 annotations. Inner-core tropical-cyclone studies use stricter time and distance filters, preferably with `S/A` scenes and high L3 valid-ocean support, because not all archive scenes sample the eye or eyewall. Coastal high-wind exposure studies can use broader storm-distance subsets when coastal distance, land fraction, valid-ocean-pixel support, and L3 masks are adequate. External wind validation uses the source-specific matchup tables and filtering procedure in Sect. 3.5, because SFMR, NDBC, and SMAP differ in sampling scale and representativeness. Statistical and machine-learning studies begin from the master scene table and use event-level or track-level grouping to avoid correlated samples and train-test leakage, especially

https://doi.org/10.5194/essd-2026-465
Preprint. Discussion started: 6 August 2026

Open Access Earth System Science Data Discussions

as AI-based ocean remote-sensing workflows increasingly depend on well-documented training data, masks, and uncertainty metadata (Li et al., 2026). L3 wind analyses apply `valid_mask` and `ocean_mask`, inspect `invalid_reason`, and avoid using unfiltered maximum wind speed as the main metric.

8 Code and data availability

The published TC-SAR-Coast v3.2 dataset is available from Zenodo at https://zenodo.org/records/20569238 and https://doi.org/10.5281/zenodo.20569238 (Zhu et al., 2026). The archived release contains the complete L0–L3 directory, validation matchup tables, a master scene table, file manifests with checksums, variable dictionaries, documentation, and user-facing scripts. The archived record distinguishes redistributed derived products from third-party source products that are referenced through provenance links only. Sentinel-1 SAR, IBTrACS, ECMWF/ERA5, GSHHG, SFMR, NDBC, and SMAP remain subject to their original provider licenses and access terms.

9 Conclusions

TC-SAR-Coast provides a global event-based Sentinel-1 SAR dataset for coastal tropical cyclones from 2015 to 2026. The v3.2 release contains 277 TC events, 411 event-track directories, and 3128 scenes organized into traceable L0–L3 layers. The dataset links SAR scene provenance, IBTrACS storm context, scene-level quality information, and the released value-added wind product in a single hierarchy. The reusable data structure and quality-aware documentation allow scenes to be selected according to storm context, coastal setting, scene usability, and product masks.

The technical assessment shows that the reported v3.2 inventory is complete at the L0–L3 level and that the released L3 wind product is suitable for quality-aware scientific use when masks and validation context are applied. SFMR validation for reference winds of at least 4 m s^{-1} gives an overall RMSE of 3.97 m s^{-1} and a small negative bias for the released approximately 1 km field, and the same matchup sample shows lower error than the ECMWF background in aircraft-sampled high-wind conditions. NDBC and SMAP comparisons provide additional point and coarse-footprint checks, with lower RMSE for the L3 product than for the ECMWF background when source-specific matchup scales are respected. The application examples further show how SAR wind scenes can be converted into reproducible high-wind footprint metrics relative to the coastline and storm-motion quadrants. These results support TC-SAR-Coast as a reusable data record for tropical-cyclone structure, coastal hazard forcing, retrieval-benchmarking, and machine-learning studies, with explicit uncertainty boundaries and recommended filters for different use cases.

Author contributions. YZ led the dataset construction, analysis workflow, figure generation, and manuscript preparation. YW, SM, YL, WL, and LR contributed to data processing, validation analysis, scientific interpretation, and manuscript revision. XL and HF supervised the study, guided the dataset design, and revised the manuscript. All authors discussed the results and contributed to the final manuscript.

Competing interests. The authors declare that they have no conflict of interest.

Financial support. This work was supported by the National Natural Science Foundation of China (Grant No. T2125006); the Guangdong Science and Technology Program (Grant No. 2025B0101080001); the Shenzhen Science and Technology Major Project for Sustainable Development (Grant No. KCXFZ20240903093759004); and the National Key Research and Development Program of China (Grant No. 2023YFB3002400).

Acknowledgements. We acknowledge the European Space Agency and the Copernicus programme for Sentinel-1 SAR data; NOAA/NCEI and the IBTrACS team for tropical-cyclone best-track records; ECMWF and the Copernicus Climate Data Store for ERA5 and related atmospheric fields; NOAA/AOML and HRD for SFMR aircraft observations; NOAA/NDBC for buoy observations; NASA/JPL and PO.DAAC for SMAP wind products; NOAA STAR for public SAR tropical-cyclone wind products used in the Delta case comparison; and Zenodo for dataset archiving.

https://doi.org/10.5194/essd-2026-465
Preprint. Discussion started: 6 August 2026

References

Alpers, W., Zhang, B., Mouche, A., Zeng, K., and Chan, P. W.: Rain footprints on C-band synthetic aperture radar images of the ocean - Revisited, Remote Sensing of Environment, 187, 169—185, https://doi.org/10.1016/j.rse.2016.10.015, 2016.

Alpers, W., Zhao, Y., Mouche, A. A., and Chan, P. W.: A note on radar signatures of hydrometeors in the melting layer as inferred from Sentinel-1 SAR data acquired over the ocean, Remote Sensing of Environment, 253, 112 177, https://doi.org/10.1016/j.rse.2020.112177, 2021.

Ardhuin, F., Chapron, B., and Collard, F.: Observation of swell dissipation across oceans, Geophysical Research Letters, 36, https://doi.org/10.1029/2008gl037030, 2009.

Avenas, A., Mouche, A., Tandeo, P., Piolle, J.-F., Chavas, D., Fablet, R., Knaff, J., and Chapron, B.: Reexamining the Estimation of Tropical Cyclone Radius of Maximum Wind from Outer Size with an Extensive Synthetic Aperture Radar Dataset, Monthly Weather Review, 151, 3169—3189, https://doi.org/10.1175/mwr-d-23-0119.1, 2023.

Avenas, A., Chapron, B., Mouche, A., Platzer, P., and Vinour, L.: Revealing short-term dynamics of tropical cyclone wind speeds from satellite synthetic aperture radar, Scientific Reports, 14, https://doi.org/10.1038/s41598-024-61384-w, 2024a.

Avenas, A., Mouche, A., Knaff, J., Carton, X., and Chapron, B.: On the Tropical Cyclone Integrated Kinetic Energy Balance, Geophysical Research Letters, 51, https://doi.org/10.1029/2024gl108327, 2024b.

Balaguru, K., Foltz, G. R., Leung, L. R., Kaplan, J., Xu, W., Reul, N., and Chapron, B.: Pronounced Impact of Salinity on Rapidly Intensifying Tropical Cyclones, Bulletin of the American Meteorological Society, 101, E1497–E1511, https://doi.org/10.1175/bams-d-19-0303.1, 2020.

Bender, M. A., Ginis, I., and Kurihara, Y.: Numerical simulations of tropical cyclone-ocean interaction with a high-resolution coupled model, Journal of Geophysical Research: Atmospheres, 98, 23 245—23 263, https://doi.org/10.1029/93jd02370, 1993.

Black, P. G., D'Asaro, E. A., Drennan, W. M., French, J. R., Niiler, P. P., Sanford, T. B., Terrill, E. J., Walsh, E. J., and Zhang, J. A.: Air–Sea Exchange in Hurricanes: Synthesis of Observations from the Coupled Boundary Layer Air–Sea Transfer Experiment, Bulletin of the American Meteorological Society, 88, 357—374, https://doi.org/10.1175/bams-88-3-357, 2007.

Chapron, B., Collard, F., and Ardhuin, F.: Direct measurements of ocean surface velocity from space: Interpretation and validation, Journal of Geophysical Research: Oceans, 110, https://doi.org/10.1029/2004jc002809, 2005.

Chavas, D. R. and Knaff, J. A.: A Simple Model for Predicting the Tropical Cyclone Radius of Maximum Wind from Outer Size, Weather and Forecasting, 37, 563—579, https://doi.org/10.1175/waf-d-21-0103.1, 2022.

Chen, X., Bryan, G. H., Zhang, J. A., Cione, J. J., and Marks, F. D.: A Framework for Simulating the Tropical-Cyclone Boundary Layer Using Large-Eddy Simulation and Its Use in Evaluating PBL Parameterizations, Journal of the Atmospheric Sciences, https://doi.org/10.1175/jas-d-20-0227.1, 2021.

Chou, K.-H., Wu, C.-C., and Lin, S.-Z.: Assessment of the ASCAT wind error characteristics by global dropwindsonde observations, Journal of Geophysical Research: Atmospheres, 118, 9011—9021, https://doi.org/10.1002/jgrd.50724, 2013.

Collard, F., Ardhuin, F., and Chapron, B.: Monitoring and analysis of ocean swell fields from space: New methods for routine observations, Journal of Geophysical Research: Oceans, 114, https://doi.org/10.1029/2008jc005215, 2009.

Combot, C., Mouche, A., Knaff, J., Zhao, Y., Zhao, Y., Vinour, L., Quilfen, Y., and Chapron, B.: Extensive High-Resolution Synthetic Aperture Radar (SAR) Data Analysis of Tropical Cyclones: Comparisons with SFMR Flights and Best Track, Monthly Weather Review, 148, 4545—4563, https://doi.org/10.1175/mwr-d-20-0005.1, 2020.

https://doi.org/10.5194/essd-2026-465
Preprint. Discussion started: 6 August 2026

Combot, C., Mouche, A., de Boyer Montegut, C., and Chapron, B.: Toward Comprehensive Understanding of Air-Sea Interactions Under Tropical Cyclones: On the Importance of High Resolution and Multi-Modal Observations, Geophysical Research Letters, 51, https://doi.org/10.1029/2024gl110637, 2024.

Dare, R. A. and McBride, J. L.: Sea Surface Temperature Response to Tropical Cyclones, Monthly Weather Review, 139, 3798—3808, https://doi.org/10.1175/mwr-d-10-05019.1, 2011.

D'Asaro, E., Black, P. G., Centurioni, L. R., Chang, Y.-T., Chen, S. S., Foster, R. C., Graber, H. C., Harr, P., Hormann, V., Lien, R.-C., Lin, I.-I., Sanford, T. B., Tang, T.-Y., and Wu, C.-C.: Impact of Typhoons on the Ocean in the Pacific, Bulletin of the American Meteorological Society, 95, 1405—1418, https://doi.org/10.1175/bams-d-12-00104.1, 2014.

Derkani, M. H., Alberello, A., Nelli, F., Bennetts, L. G., Hessner, K. G., MacHutchon, K., Reichert, K., Aouf, L., Khan, S., and Toffoli, A.: Wind, waves, and surface currents in the Southern Ocean: observations from the Antarctic Circumnavigation Expedition, Earth System Science Data, 13, 1189—1209, https://doi.org/10.5194/essd-13-1189-2021, 2021.

Duong, Q.-P., Langlade, S., Payan, C., Husson, R., Mouche, A., and Malardel, S.: C-Band SAR Winds for Tropical Cyclone Monitoring and Forecast in the South-West Indian Ocean, Atmosphere, 12, 576, https://doi.org/10.3390/atmos12050576, 2021.

Emanuel, K. A.: An Air-Sea Interaction Theory for Tropical Cyclones. Part I: Steady-State Maintenance, Journal of the Atmospheric Sciences, 43, 585—605, https://doi.org/10.1175/1520-0469(1986)043<0585:aasitf>2.0.co;2, 1986.

Engen, G. and Johnsen, H.: SAR-ocean wave inversion using image cross spectra, IEEE Transactions on Geoscience and Remote Sensing, 33, 1047—1056, https://doi.org/10.1109/36.406690, 1995.

Fan, S., Zhang, B., Mouche, A. A., Perrie, W., Zhang, J. A., and Zhang, G.: Estimation of Wind Direction in Tropical Cyclones Using C-Band Dual-Polarization Synthetic Aperture Radar, IEEE Transactions on Geoscience and Remote Sensing, 58, 1450—1462, https://doi.org/10.1109/tgrs.2019.2946885, 2020.

Fernandez, D., Kerr, E., Castells, A., Carswell, J., Frasier, S., Chang, P., Black, P., and Marks, F.: IWRAP: the Imaging Wind and Rain Airborne Profiler for remote sensing of the ocean and the atmospheric boundary layer within tropical cyclones, IEEE Transactions on Geoscience and Remote Sensing, 43, 1775—1787, https://doi.org/10.1109/tgrs.2005.851640, 2005.

Fore, A. G., Yueh, S. H., Stiles, B. W., Tang, W., and Hayashi, A. K.: SMAP Radiometer-Only Tropical Cyclone Intensity and Size Validation, IEEE Geoscience and Remote Sensing Letters, 15, 1480—1484, https://doi.org/10.1109/lgrs.2018.2849649, 2018.

Gourmelon, N., Seehaus, T., Braun, M., Maier, A., and Christlein, V.: Calving fronts and where to find them: a benchmark dataset and methodology for automatic glacier calving front extraction from synthetic aperture radar imagery, Earth System Science Data, 14, 4287—4313, https://doi.org/10.5194/essd-14-4287-2022, 2022.

Hersbach, H., Stoffelen, A., and de Haan, S.: An improved C-band scatterometer ocean geophysical model function: CMOD5, Journal of Geophysical Research: Oceans, 112, https://doi.org/10.1029/2006jc003743, 2007.

Hersbach, H., Bell, B., Berrisford, P., Hirahara, S., Horanyi, A., Munoz-Sabater, J., Nicolas, J., Peubey, C., Radu, R., Schepers, D., Simmons, A., Soci, C., Abdalla, S., Abellan, X., Balsamo, G., Bechtold, P., Biavati, G., Bidlot, J., Bonavita, M., De Chiara, G., Dahlgren, P., Dee, D., Diamantakis, M., Dragani, R., Flemming, J., Forbes, R., Fuentes, M., Geer, A., Haimberger, L., Healy, S., Hogan, R. J., Holm, E., Janiskova, M., Keeley, S., Laloyaux, P., Lopez, P., Lupu, C., Radnoti, G., de Rosnay, P., Rozum, I., Vamborg, F., Villaume, S., and Thepaut, J.-N.: The ERA5 global reanalysis, Quarterly Journal of the Royal Meteorological Society, 146, 1999—2049, https://doi.org/10.1002/qj.3803, 2020.

Holland, G. J.: An Analytic Model of the Wind and Pressure Profiles in Hurricanes, Monthly Weather Review, 108, 1212—1218, https://doi.org/10.1175/1520-0493(1980)108<1212:aamotw>2.0.co;2, 1980.

Kleinherenbrink, M., Lopez-Dekker, P., Nouguier, F., and Chapron, B.: Bistatic SAR Mapping of Ocean-Wave Spectra, IEEE Transactions on Geoscience and Remote Sensing, 62, 1—12, https://doi.org/10.1109/tgrs.2024.3394245, 2024.

Klotz, B. W. and Uhlhorn, E. W.: Improved Stepped Frequency Microwave Radiometer Tropical Cyclone Surface Winds in Heavy Precipitation, Journal of Atmospheric and Oceanic Technology, 31, 2392—2408, https://doi.org/10.1175/jtech-d-14-00028.1, 2014.

Knapp, K. R., Kruk, M. C., Levinson, D. H., Diamond, H. J., and Neumann, C. J.: The International Best Track Archive for Climate Stewardship (IBTrACS): Unifying Tropical Cyclone Data, Bulletin of the American Meteorological Society, 91, 363—376, https://doi.org/10.1175/2009bams2755.1, 2010.

Li, X., Pichel, W. G., He, M., Wu, S., Friedman, K. S., Clemente-Colon, P., and Zhao, C.: Observation of Hurricane-Generated Ocean Swell Refraction at the Gulf Stream North Wall with the RADARSAT-1 Synthetic Aperture Radar, IEEE Transactions on Geoscience and Remote Sensing, 40, 2131—2142, https://doi.org/10.1109/TGRS.2002.802474, 2002.

Li, X., Zhang, B., and Yang, X.: Remote Sensing of Sea-Surface Wind and Wave from Spaceborne Synthetic Aperture Radar, Journal of Radars, 9, 425—443, https://doi.org/10.12000/JR20079, 2020.

Li, X., Xu, Q., Wang, H., Jiang, H., Yin, X., Mu, S., Li, X., Su, H., Wang, A., Yang, Y., Wang, Y., Ren, Y., Zhang, X., Liu, Y., and Wang, C.: AI in Satellite Remote Sensing of the Ocean, Proceedings of the IEEE, pp. 1—34, https://doi.org/10.1109/JPROC.2026.3664121, 2026.

Liu, B., Li, X., and Zheng, G.: Coastal Inundation Mapping From Bitemporal and Dual-Polarization SAR Imagery Based on Deep Convolutional Neural Networks, Journal of Geophysical Research: Oceans, 124, 9101—9113, https://doi.org/10.1029/2019jc015577, 2019.

Longepe, N., Mouche, A. A., Ferro-Famil, L., and Husson, R.: Co-Cross-Polarization Coherence Over the Sea Surface From Sentinel-1 SAR Data: Perspectives for Mission Calibration and Wind Field Retrieval, IEEE Transactions on Geoscience and Remote Sensing, 60, 1—16, https://doi.org/10.1109/tgrs.2021.3055979, 2022.

Manaster, A., Ricciardulli, L., and Meissner, T.: Tropical Cyclone Winds from WindSat, AMSR2, and SMAP: Comparison with the HWRF Model, Remote Sensing, 13, 2347, https://doi.org/10.3390/rs13122347, 2021.

Mouche, A., Avenas, A., Chang, P., Chapron, B., Cevaer, T., Combot, C., Courtney, J., Febvre, Q., Foster, R. C., Grouazel, A., Hayashi, M., Horinouchi, T., Ikuta, Y., Isoguchi, O., Jackson, C. R., Jelenak, Z., Knaff, J. A., Langlade, S., Miadana, J.-R., Nouguier, F., Ohki, M., Pouplin, C., Ruff, T. W., Sampson, C. R., Sapp, J., Shimada, U., Tadono, T., Tsukada, T., and Vinour, L.: Fostering tropical cyclone research and applications with Synthetic Aperture Radar, Remote Sensing of Environment, 333, 115 139, https://doi.org/10.1016/j.rse.2025.115139, 2026.

Ni, W., Stoffelen, A., Ren, K., Yang, X., and Vogelzang, J.: SAR and ASCAT Tropical Cyclone Wind Speed Reconciliation, Remote Sensing, 14, 5535, https://doi.org/10.3390/rs14215535, 2022.

Ni, W., Stoffelen, A., Ren, K., Vogelzang, J., Zhao, Y., Yang, X., and Wang, W.: Enhanced Tropical Cyclone ASCAT Winds Guided by SAR-Learned Spatial Structure Functions, IEEE Transactions on Geoscience and Remote Sensing, 63, 1—19, https://doi.org/10.1109/tgrs.2024.3516209, 2025.

NOAA STAR: SAR Tropical Cyclone Winds, `https://www.star.nesdis.noaa.gov/socd/mecb/sar/sarwinds_tropical.php`, nOAA Center for Satellite Applications and Research, accessed 3 June 2026, 2026.

Pouplin, C., Mouche, A., and Chapron, B.: A Multi-Sensor Approach for the Characterization of Tropical Cyclone Induced Swell–Application to TC Larry, 2021, Geophysical Research Letters, 51, https://doi.org/10.1029/2024gl109712, 2024.

Quach, B., Glaser, Y., Stopa, J. E., Mouche, A. A., and Sadowski, P.: Deep Learning for Predicting Significant Wave Height From Synthetic Aperture Radar, IEEE Transactions on Geoscience and Remote Sensing, 59, 1859—1867, https://doi.org/10.1109/tgrs.2020.3003839, 2021.

https://doi.org/10.5194/essd-2026-465
Preprint. Discussion started: 6 August 2026

Ribal, A. and Young, I. R.: 33 years of globally calibrated wave height and wind speed data based on altimeter observations, Scientific Data, 6, https://doi.org/10.1038/s41597-019-0083-9, 2019.

Shao, W., Hu, Y., Zou, Q., Migliaccio, M., and Jiang, X.: Asymmetry of Cyclonic Sea Surface Wind and Wave Observed by SAR, Geophysical Research Letters, 52, https://doi.org/10.1029/2025gl116600, 2025.

Stoffelen, A., Verspeek, J. A., Vogelzang, J., and Verhoef, A.: The CMOD7 Geophysical Model Function for ASCAT and ERS Wind Retrievals, IEEE Journal of Selected Topics in Applied Earth Observations and Remote Sensing, 10, 2123—2134, https://doi.org/10.1109/jstars.2017.2681806, 2017.

Torres, R., Snoeij, P., Geudtner, D., Bibby, D., Davidson, M., Attema, E., Potin, P., Rommen, B., Floury, N., Brown, M., Traver, I. N., Deghaye, P., Duesmann, B., Rosich, B., Miranda, N., Bruno, C., L'Abbate, M., Croci, R., Pietropaolo, A., Huchler, M., and Rostan, F.: GMES Sentinel-1 mission, Remote Sensing of Environment, 120, 9—24, https://doi.org/10.1016/j.rse.2011.05.028, 2012.

Uhlhorn, E. W., Black, P. G., Franklin, J. L., Goodberlet, M., Carswell, J., and Goldstein, A. S.: Hurricane Surface Wind Measurements from an Operational Stepped Frequency Microwave Radiometer, Monthly Weather Review, 135, 3070—3085, https://doi.org/10.1175/mwr3454.1, 2007.

Wang, S., Yuen, K.-V., Yang, X., and Zhang, B.: A Nonparametric Tropical Cyclone Wind Speed Estimation Model Based on Dual-Polarization SAR Observations, IEEE Transactions on Geoscience and Remote Sensing, 60, 1—13, https://doi.org/10.1109/tgrs.2022.3188328, 2022.

Wang, Y.-R. and Li, X.-M.: Arctic sea ice cover data from spaceborne synthetic aperture radar by deep learning, Earth System Science Data, 13, 2723—2742, https://doi.org/10.5194/essd-13-2723-2021, 2021.

Wessel, P. and Smith, W. H. F.: A global, self-consistent, hierarchical, high-resolution shoreline database, Journal of Geophysical Research: Solid Earth, 101, 8741—8743, https://doi.org/10.1029/96jb00104, 1996.

Xu, Z., Guo, J., Zhang, G., Ye, Y., Zhao, H., and Chen, H.: Global tropical cyclone size and intensity reconstruction dataset for 1959–2022 based on IBTrACS and ERA5 data, Earth System Science Data, 16, 5753—5766, https://doi.org/10.5194/essd-16-5753-2024, 2024.

Yang, Y.-J., Singha, S., Goldman, R., and Schutte, F.: Dataset of oil slicks, look-alikes and remarkable SAR signatures obtained from Sentinel-1 data in the Eastern Mediterranean Sea, Earth System Science Data, 17, 6807—6837, https://doi.org/10.5194/essd-17-6807-2025, 2025.

Zhang, B., Wen, L., Perrie, W., and Kudryavtsev, V.: Sea Surface Height Response to Tropical Cyclone From Satellite Altimeter Observations and SAR Estimates, IEEE Transactions on Geoscience and Remote Sensing, 62, 1—9, https://doi.org/10.1109/tgrs.2024.3371168, 2024.

Zhang, G., Zhang, B., Perrie, W., Xu, Q., and He, Y.: A Hurricane Tangential Wind Profile Estimation Method for C-Band Cross-Polarization SAR, IEEE Transactions on Geoscience and Remote Sensing, 52, 7186—7194, https://doi.org/10.1109/tgrs.2014.2308839, 2014.

Zhang, G., Li, X., Perrie, W., and Zhang, J. A.: Tropical Cyclone Winds and Inflow Angle Asymmetry From SAR Imagery, Geophysical Research Letters, 48, https://doi.org/10.1029/2021gl095699, 2021.

Zhu, Y., Grieco, G., Lin, J., Portabella, M., and Wang, X.: On the Use of Azimuth Cutoff for Sea Surface Wind Speed Retrieval From SAR, IEEE Journal of Selected Topics in Applied Earth Observations and Remote Sensing, 17, 10 367—10 379, https://doi.org/10.1109/JSTARS.2024.3407115, 2024.

Zhu, Y., Wang, Y., Mu, S., Li, X., Liu, Y., Li, W., Fan, S., and Fu, H.: TC-SAR-Coast: an event-based Sentinel-1 SAR dataset with high-resolution wind fields for coastal tropical cyclones, https://doi.org/10.5281/zenodo.20569238, dataset, 2026.